



Calhoun: The NPS Institutional Archive DSpace Repository

Theses and Dissertations

1. Thesis and Dissertation Collection, all items

2005-09

Experimental and computational investigation of flow in a transonic compressor inlet

Brunner, Matthew D.

Monterey, California. Naval Postgraduate School

<http://hdl.handle.net/10945/2022>

This publication is a work of the U.S. Government as defined in Title 17, United States Code, Section 101. Copyright protection is not available for this work in the United States.

Downloaded from NPS Archive: Calhoun



<http://www.nps.edu/library>

Calhoun is the Naval Postgraduate School's public access digital repository for research materials and institutional publications created by the NPS community.

Calhoun is named for Professor of Mathematics Guy K. Calhoun, NPS's first appointed -- and published -- scholarly author.

Dudley Knox Library / Naval Postgraduate School
411 Dyer Road / 1 University Circle
Monterey, California USA 93943



**NAVAL
POSTGRADUATE
SCHOOL**

MONTEREY, CALIFORNIA

THESIS

**EXPERIMENTAL AND COMPUTATIONAL
INVESTIGATION OF FLOW IN A TRANSONIC
COMPRESSOR INLET**

by

Matthew D. Brunner

September 2005

Thesis Advisor:
Second Reader:

Garth V. Hobson
Raymond P. Shreeve

Approved for public release; distribution is unlimited

THIS PAGE INTENTIONALLY LEFT BLANK

REPORT DOCUMENTATION PAGE

Form Approved OMB No. 0704-0188

Public reporting burden for this collection of information is estimated to average 1 hour per response, including the time for reviewing instruction, searching existing data sources, gathering and maintaining the data needed, and completing and reviewing the collection of information. Send comments regarding this burden estimate or any other aspect of this collection of information, including suggestions for reducing this burden, to Washington Headquarters Services, Directorate for Information Operations and Reports, 1215 Jefferson Davis Highway, Suite 1204, Arlington, VA 22202-4302, and to the Office of Management and Budget, Paperwork Reduction Project (0704-0188) Washington DC 20503.

1. AGENCY USE ONLY (<i>Leave blank</i>)	2. REPORT DATE September 2005	3. REPORT TYPE AND DATES COVERED Master's Thesis
4. TITLE AND SUBTITLE: Experimental and Computational Investigation of Flow in a Transonic Compressor Inlet		5. FUNDING NUMBERS
6. AUTHOR(S) Matthew D. Brunner		
7. PERFORMING ORGANIZATION NAME(S) AND ADDRESS(ES) Naval Postgraduate School Monterey, CA 93943-5000		8. PERFORMING ORGANIZATION REPORT NUMBER
9. SPONSORING /MONITORING AGENCY NAME(S) AND ADDRESS(ES) N/A		10. SPONSORING/MONITORING AGENCY REPORT NUMBER
11. SUPPLEMENTARY NOTES The views expressed in this thesis are those of the author and do not reflect the official policy or position of the Department of Defense or the U.S. Government.		
12a. DISTRIBUTION / AVAILABILITY STATEMENT Approved for public release; distribution is unlimited		12b. DISTRIBUTION CODE
13. ABSTRACT (maximum 200 words) As part of an initial baseline survey of the inlet flow-field into a transonic compressor rotor, a five-hole probe was calibrated and used to determine the Mach number and inlet pitch angle distributions. The data for Mach number were compared to data obtained with a three-hole probe. A numerical investigation of the flow in the inlet ducting to the rotor was also initiated using the commercial code CFX marketed by ANSYS. Comparisons were also made between the numerical predictions and the experimental measurements. The purpose of the study was to more accurately determine the characteristics of the flow to the rotor of the compressor prior to steam-ingestion experiments to quantify effects on compressor stability.		
14. SUBJECT TERMS Compressor, Transonic, Steam Ingestion, Inlet Distortion, Computational Fluid Dynamics, Multiphase Flow		15. NUMBER OF PAGES 83
		16. PRICE CODE
17. SECURITY CLASSIFICATION OF REPORT Unclassified	18. SECURITY CLASSIFICATION OF THIS PAGE Unclassified	19. SECURITY CLASSIFICATION OF ABSTRACT Unclassified
		20. LIMITATION OF ABSTRACT UL

NSN 7540-01-280-5500

Standard Form 298 (Rev. 2-89)
Prescribed by ANSI Std. Z39-18

THIS PAGE INTENTIONALLY LEFT BLANK

Approved for public release; Distribution is unlimited

**EXPERIMENTAL AND COMPUTATIONAL INVESTIGATION OF
FLOW IN A TRANSONIC COMPRESSOR INLET**

Matthew D. Brunner
Ensign, United States Navy Reserve
B.S., United States Naval Academy, 2004

Submitted in partial fulfillment of the
requirements for the degree of

MASTER OF SCIENCE IN MECHANICAL ENGINEERING

from the

**NAVAL POSTGRADUATE SCHOOL
September 2005**

Author: Matthew D. Brunner

Approved by: Garth Hobson
Thesis Advisor

Raymond Shreeve
Second Reader

Anthony J. Healey
Chairman, Department of Mechanical and Astronautical
Engineering

THIS PAGE INTENTIONALLY LEFT BLANK

ABSTRACT

As part of an initial baseline survey of the inlet flow-field into a transonic compressor rotor, a five-hole probe was calibrated and used to determine the Mach number and inlet pitch angle distributions. The data for Mach number were compared to data obtained with a three-hole probe. A numerical investigation of the flow in the inlet ducting to the rotor was also initiated using the commercial code CFX marketed by ANSYS. Comparisons were also made between the numerical predictions and the experimental measurements. The purpose of the study was to more accurately determine the characteristics of the flow to the rotor of the compressor prior to steam-ingestion experiments to quantify effects on compressor stability.

THIS PAGE INTENTIONALLY LEFT BLANK

TABLE OF CONTENTS

I.	INTRODUCTION	1
II.	EXPERIMENTAL TESTING FACILITIES AND EQUIPMENT.....	3
A.	TRANSONIC COMPRESSOR RIG	3
1.	Sanger Rotor	4
2.	Compressor Inlet and Case Wall	4
B.	FREE-JET TEST FACILITY	5
III.	INSTRUMENTATION	7
A.	PROBES	7
B.	PROBE ACTUATOR	8
C.	OMEGA PX-138 PRESSURE TRANSDUCERS.....	9
D.	USB ERB-24 REMOTE RELAY CONTROLLER	10
E.	PMD-1608FS ANALOG AND DIGITAL I/O MODULE	10
F.	MATLAB 6.5 R13	13
IV.	FREE-JET CALIBRATION	15
A.	PURPOSE.....	15
B.	PROCEDURE	15
C.	DATA COLLECTION.....	16
D.	CALIBRATION EQUATIONS	16
E.	CALIBRATION RESULTS.....	17
V.	TRANSONIC COMPRESSOR RIG EXPERIMENTATION	21
A.	PROCEDURE	21
B.	EXPERIMENTAL RESULTS.....	22
VI.	CFD MODELLING	27
A.	DESCRIPTION OF CODES	27
1.	ICEM CFD.....	27
2.	CFX-5.....	27
B.	CFD MODELS	28
1.	Air Inlet Duct.....	28
2.	Inlet Distortion Duct.....	29
3.	Inlet Bell-Mouth.....	30
C.	CFD MACH NUMBER CALCULATION RESULTS	30
VII.	COMPARISON OF RESULTS.....	33
VIII.	CONCLUSION	37
IX.	RECOMMENDATIONS.....	39
	LIST OF REFERENCES.....	41
	APPENDIX A – TRANSONIC COMPRESSOR RIG SETUP	43

APPENDIX B – CASE WALL SCHEMATIC.....	45
APPENDIX C – MATLAB SOURCE CODE	47
APPENDIX C-1 - PMD_1608FS_3_1.M.....	47
APPENDIX C-2 - PMD_1608FS_3_2.M.....	48
APPENDIX C-3 - PRESSURE_CALIBRATION_1.M	49
APPENDIX C-4 - PRESSURE_CALIBRATION_2.M	51
APPENDIX C-5 - OUTPUT_TO_EXCEL.M.....	53
APPENDIX D – OPEN-THROTTLE RAW DATA.....	59
APPENDIX D-1 – 30% DESIGN SPEED.....	59
APPENDIX D-2 – 40% DESIGN SPEED.....	59
APPENDIX D-3 – 50% DESIGN SPEED.....	59
APPENDIX D-4 – 60% DESIGN SPEED.....	60
APPENDIX D-5 – 70% DESIGN SPEED.....	60
APPENDIX D-6 – 80% DESIGN SPEED.....	60
APPENDIX D-7 – 90% DESIGN SPEED.....	61
APPENDIX D-8 – 100% DESIGN SPEED.....	61
APPENDIX E – INLET DISTORTION SCHEMATIC	63
APPENDIX F – MULTI-PHASE FLOW EXAMPLE.....	65
INITIAL DISTRIBUTION LIST	67

LIST OF FIGURES

Figure 1.	Transonic Compressor Rig	3
Figure 2.	The Sanger rotor.....	4
Figure 3.	Compressor case wall	5
Figure 4.	Dropped top plate.....	5
Figure 5.	Free-jet.....	6
Figure 6.	Five-hole probe	7
Figure 7.	Five-hole probe schematic	7
Figure 8.	L.C. Smith probe actuator mounted on the free-jet rig	8
Figure 9.	Omega PX-138 series pressure transducer	9
Figure 10.	USB ERB-24 remote relay controller	10
Figure 11.	PMD-1608FS analog and digital I/O module	11
Figure 12.	Wiring diagram for probe transducer acquisition	12
Figure 13.	Beta vs. yaw angle and Mach number calibration plot	18
Figure 14.	Gamma vs. pitch angle and Mach number calibration plot.....	18
Figure 15.	Mach number distribution at open throttle conditions	22
Figure 16.	Mach number distribution at 70% design speed conditions	23
Figure 17.	Mach number distribution at 90% design speed conditions	24
Figure 18.	Magnitude of the flow pitch towards the centerline.....	25
Figure 19.	Air inlet duct CFD model	28
Figure 20.	Inlet distortion duct CFD model	29
Figure 21.	Inlet bell-mouth grid.....	30
Figure 22.	Comparison of five-hole and three-hole probe data.....	33
Figure 23.	Open-throttle Mach number distribution comparison.....	34
Figure 24.	70% design speed Mach number distribution comparison	35
Figure 25.	90% design speed Mach number distribution comparison.....	36

THIS PAGE INTENTIONALLY LEFT BLANK

LIST OF TABLES

Table 1.	Calibration nomenclature	17
Table 2.	Sampling positions.....	21
Table 3.	Boundary conditions used in each CFD model	31

THIS PAGE INTENTIONALLY LEFT BLANK

ACKNOWLEDGMENTS

The most important thing is to thank everyone who helped me out along the way. I sincerely appreciate the help of everyone at the Turbopropulsion Lab. Each and every one made it an excellent environment to work in every day.

Specifically, I would like to thank Professor Garth Hobson for allowing me to complete this research and for helping me out along the way. His guidance was immeasurable and always greatly appreciated.

I would also like to thank Dr. Anthony Gannon for all of the help gave me. His extensive knowledge made it possible to quickly troubleshoot any experimental problem at hand, making it possible to complete the present work on time.

I would also like to thank Professor Raymond Shreeve for his help in correcting the numerous mistakes I made along the way.

Finally I would like to thank Rick Still and John Gibson for constantly helping me fix the little problems that kept arising as well as keeping me grounded when I got too lost in the work.

Very special thanks to everyone for providing an enjoyable place to work and learn. Hopefully we will have the chance to work together again.

THIS PAGE INTENTIONALLY LEFT BLANK

I. INTRODUCTION

Currently at the Turbopropulsion Laboratory (TPL) at the Naval Postgraduate School (NPS) a study is underway in order to determine and evaluate the effects and causes of “pop stalls” caused by steam ingestion by aircraft engines during catapult launches from US Navy carriers. This particular subject is of great importance as the US Navy is transitioning to the F-35C, Joint Strike Fighter (JSF), aircraft. The US Navy currently has an inventory of dual-engine aircraft which may mitigate the catastrophic effects of “pop stalls” on launch; however, the F-35C is powered by a single Pratt & Whitney F-135 engine, which makes it potentially susceptible to “pop stall” problems. Although different from the General Electric F404/414 currently used on the F-18 fighter aircraft, the problem must be thoroughly understood in order to minimize the possibility of engine failure in a single engine aircraft. (Donelson, 2003)

The initial steps in of the NPS program are first to analyze and evaluate the flow-field into a transonic compressor and then to generate conditions similar to catapult-assisted take-off in order to evaluate the effects of steam on the compressor stability. Understanding the effects of steam on the fan and compressor are necessary steps toward understanding the overall pop-stall problem. The first stage of the present study will use a small-scale transonic compressor test rig. The highly loaded single axial stage to be used in the experiments was designed by Nelson Sanger at the NASA Lewis Research Center in 1996 and has been extensively tested at TPL. (Gannon, Hobson, & Shreeve, 2005) The Sanger rotor is a low aspect ratio transonic design which was developed using CFD modeling. (Sanger, 1996)

Following performance measurements using fixed instrumentation, flow-field surveys were conducted upstream and downstream of the single rotor using a three-hole pressure probe. Data were obtained at 70, 80, 90, and 100 percent of design speed with mass flow rates varying from open-throttle to peak-efficiency and near-stall conditions. (Villegas, 2005) Following the recommendations of the prior study, a five-hole probe was used in the present work to obtain flow-field surveys upstream of the rotor at the 70, 90, and 100 percent design speed at open throttle conditions as well as at peak-efficiency

and near-stall conditions. The five-hole probe determined pitch angle, which the three-hole probe could not, but the Mach numbers obtained were compared to the three-hole probe data.

The present study also included the development of CFD models for the air inlet duct leading to the inlet of the compressor, the inlet bell-mouth of the compressor, and a special inlet duct that allowed for the addition of steam into the flow. Using the data from the three-hole probe, the five-hole probe, and the CFD models a detailed comparison of experimental and analytical results was made. From these comparisons an evaluation of the CFD code could be made prior to initiating a study of the effects of steam injected into the flow.

II. EXPERIMENTAL TESTING FACILITIES AND EQUIPMENT

The current research was conducted on the transonic compressor rig at the Turbopropulsion Laboratory at M.H. Vavra Aero-Propulsion Laboratories within the Department of Mechanical Engineering at the Naval Postgraduate School.

A. TRANSONIC COMPRESSOR RIG

The transonic compressor rig (TCR), shown in Figure 1, was originally designed by Professor Michael Vavra in order to test a transonic compressor stage. The TCR was driven by two opposed-rotor air turbine stages, supplied by an Allis-Chalmers axial compressor. This compressor supplied air pressure up to 30 pounds per square inch gauge, at a flow rate up to 11 pounds per second. The test compressor was recommissioned in 2000 by Joseph O'Brien following a failure of the original Sanger rotor in 1997. A schematic of the test facility is presented in Appendix A. (O'Brien, 2000)

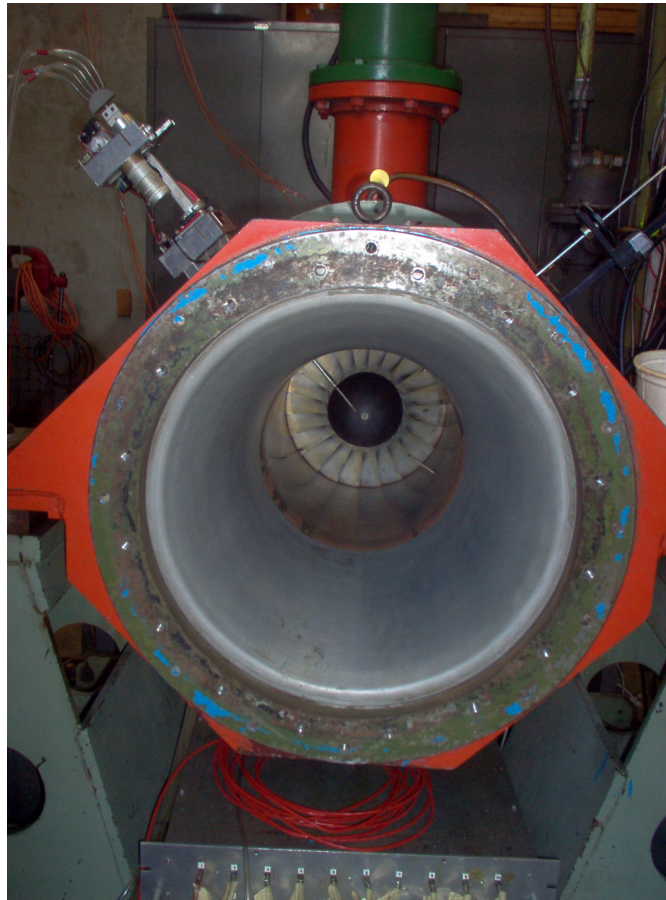


Figure 1. Transonic Compressor Rig

1. Sanger Rotor

The transonic compressor rotor, displayed in Figure 2, was designed as part of a fan stage by Sanger for use by the NPS Turbopropulsion Laboratory (TPL) using the Denton CFD code. It consisted of 22 blades manufactured from high strength aluminum (7075-T6) alloy. (O'Brien, 2000) For the present experiment the rotor assembly utilized a parabolic spinner. (Gannon, et. al., 2005)

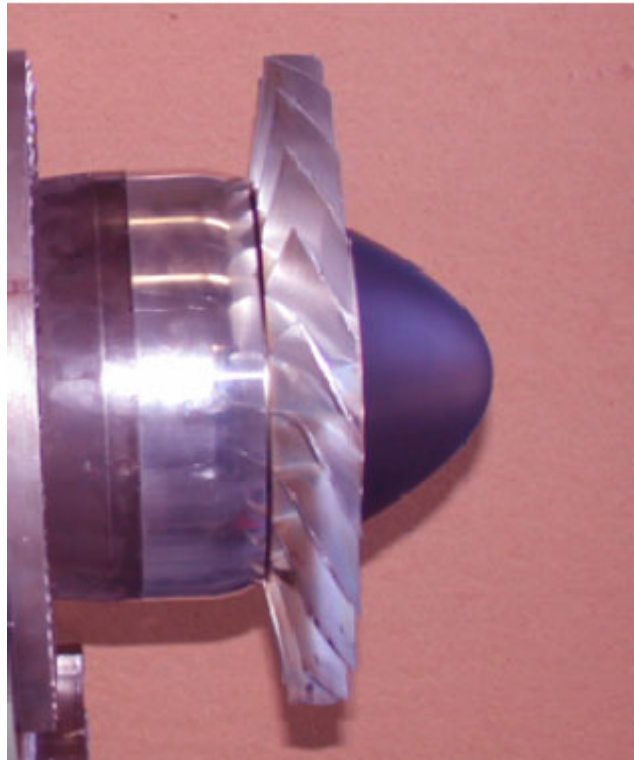


Figure 2. The Sanger rotor

2. Compressor Inlet and Case Wall

The compressor inlet assembly consisted of an elliptic bell-mouth and a steel case wall for mounting instrumentation. The bell-mouth was 59cm long and converged from a diameter of 45.8cm to a diameter of 27.9cm. The case wall was a steel duct over the whole rotor with holes drilled and tapped, in order to mount instrumentation. There were four holes bored into the case wall in order to insert a probe into the flow, displayed and numbered in Figure 3. The hole marked number 1 was located approximately 2.5cm upstream of the tip of the rotor spinner. This hole was the specific point used for the insertion of the test probe. Further details of the case wall can be found in Appendix B.

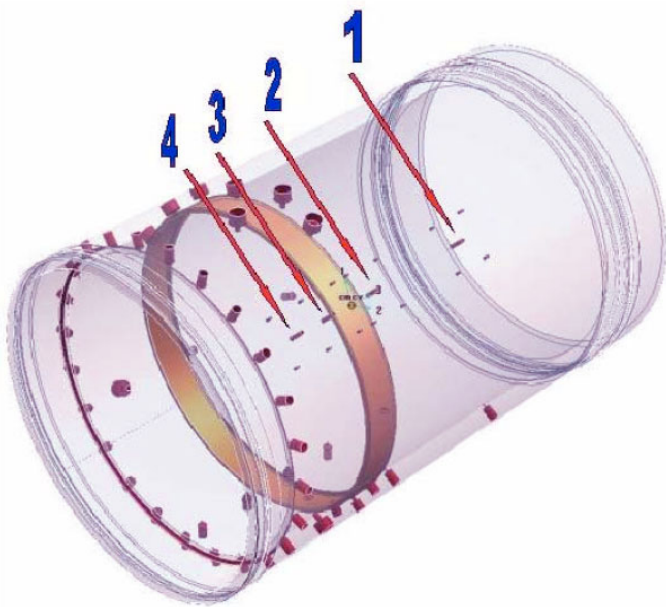


Figure 3. Compressor case wall

B. FREE-JET TEST FACILITY

The free-jet test facility was used for the calibration of the five-hole probe. Because of the length of the five-hole probe, a specially constructed top plate was created out of $\frac{1}{4}$ inch aluminum for the free-jet instrumentation rig, displayed in Figure 4.

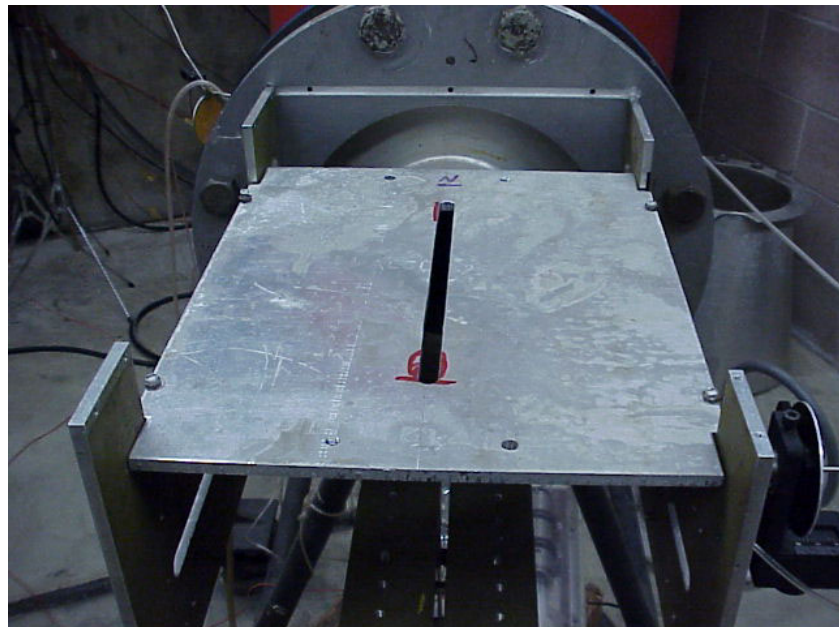


Figure 4. Dropped top plate

The specially constructed top plate dropped the height of the top of the rig approximately 3.8cm. Mounted to the top of this plate was an adjustable pitch bracket, to which the five-hole probe was attached.

The free-jet was a 10.8cm nozzle opening to the atmosphere and utilized compressed air from the Allis-Chalmers compressor. For flow Mach numbers of 0.85 to 0.3, a dump valve on the compressor was throttled. For flow Mach numbers of 0.3 to 0.15, a manual shut off valve in the free-jet cell was closed by hand. The free-jet assembly with probes positioned is shown in Figure 5.

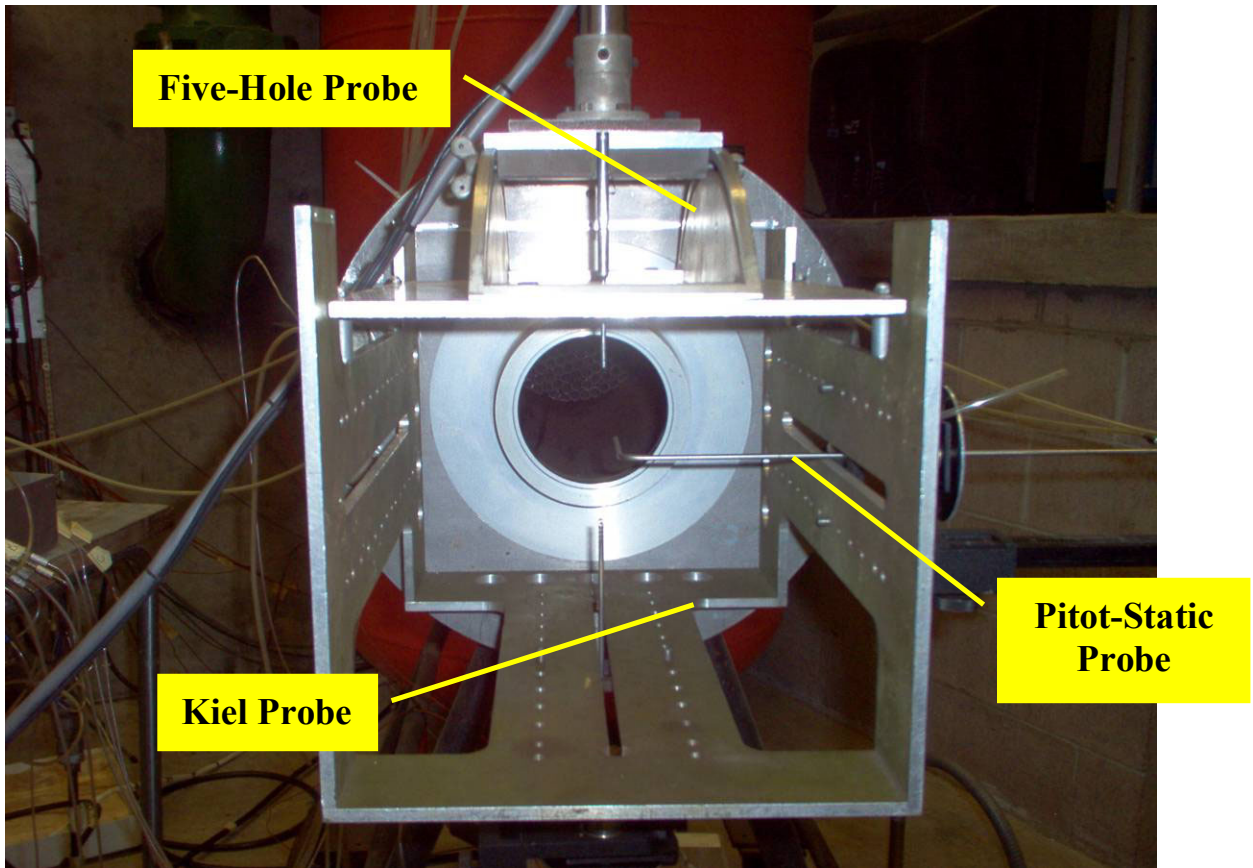


Figure 5. Free-jet

III. INSTRUMENTATION

A. PROBES

The main test probe for the experiment was a standard five-hole probe shown in Figure 6.



Figure 6. Five-hole probe

The layout of the pressure ports is displayed in the sketch below, Figure 7.
(Anderson, Olsen, Shreeve, 1977)

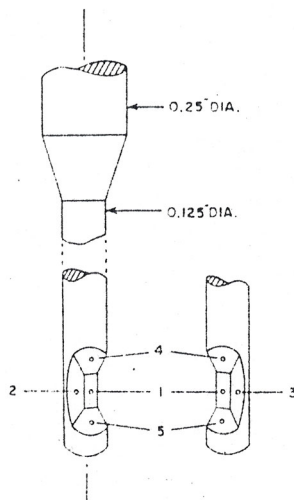


Figure 7. Five-hole probe schematic

Two additional probes were used in the free-jet calibrations and the experiments, a kiel probe to measure stagnation pressure and a pitot-static probe to detect static pressure.

B. PROBE ACTUATOR

Before calibration or application, the five-hole probe used was mounted into the L.C. Smith probe actuator, shown below in Figure 8.



Figure 8. L.C. Smith probe actuator mounted on the free-jet rig

The probe actuator had two electric motors that controlled the rotation and radial traverse of the probe into the flow. The setup of the probe actuator and the PC control board was the same as described by Villescas. (Villescas, 2005)

C. OMEGA PX-138 PRESSURE TRANSDUCERS

The Omega PX-138 series of pressure transducers use “state-of-the-art micromachined silicon pressure sensors” which were able to sense the relative pressure changes and represent them as voltages. A photograph of one of the transducers is shown in Figure 9.

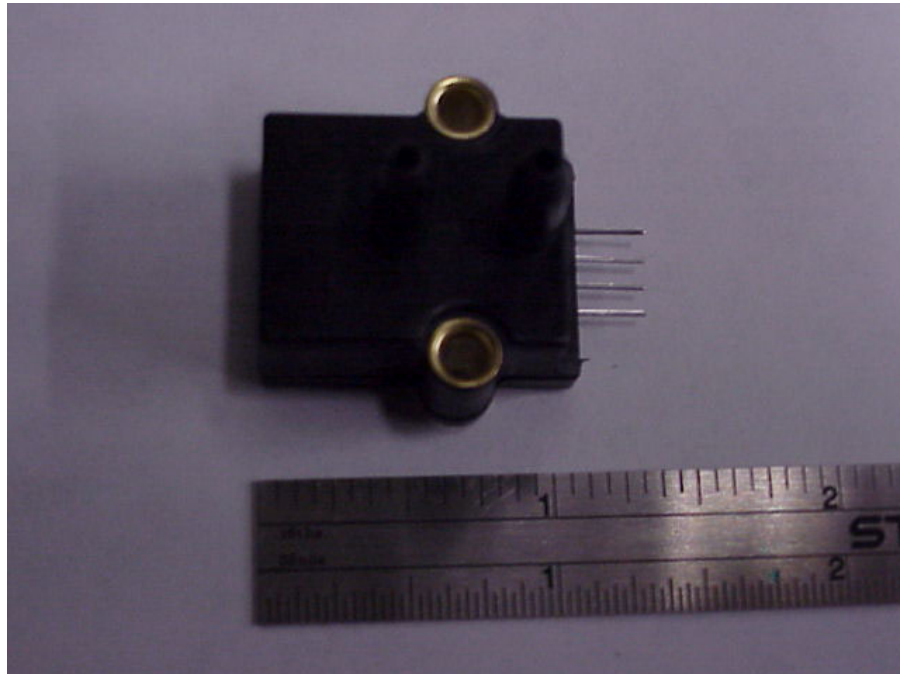


Figure 9. Omega PX-138 series pressure transducer

The specific transducers used were the PX138-015D5V model, which were able to detect a differential pressure of ± 15 PSI with a maximum error of $\pm 0.5\%$. (Omega, 2005) A total of seven pressure transducers were used either in the free-jet facility or in the TCR, five for each pressure port on the probe and two for static and stagnation pressure mounted in the facility. Each transducer was individually calibrated using known pressures.

Each of the seven pressure transducers was connected to a regulated 8VDC power supply. Improvements on the power supply box and transducer connections were made from the previous setup by Villescas. (Villescas, 2005) The CX-136-4 plastic connectors were replaced with off-the-shelf, four-pin connectors which improved electrical connectivity. Also the wiring of the power supply and signal output were modified to allow for removal and electrical testing of individual transducers. Finally,

the amount of excess wiring was reduced in order to minimize any electrical line loss or added resistance. The new wiring proved to be more robust and never resulted in any problems with electrical connectivity.

D. USB ERB-24 REMOTE RELAY CONTROLLER

The USB ERB-24 Remote Relay Controller was a USB control device connected to a PC and was used to control the L.C. Smith probe actuator, shown below in Figure 10.

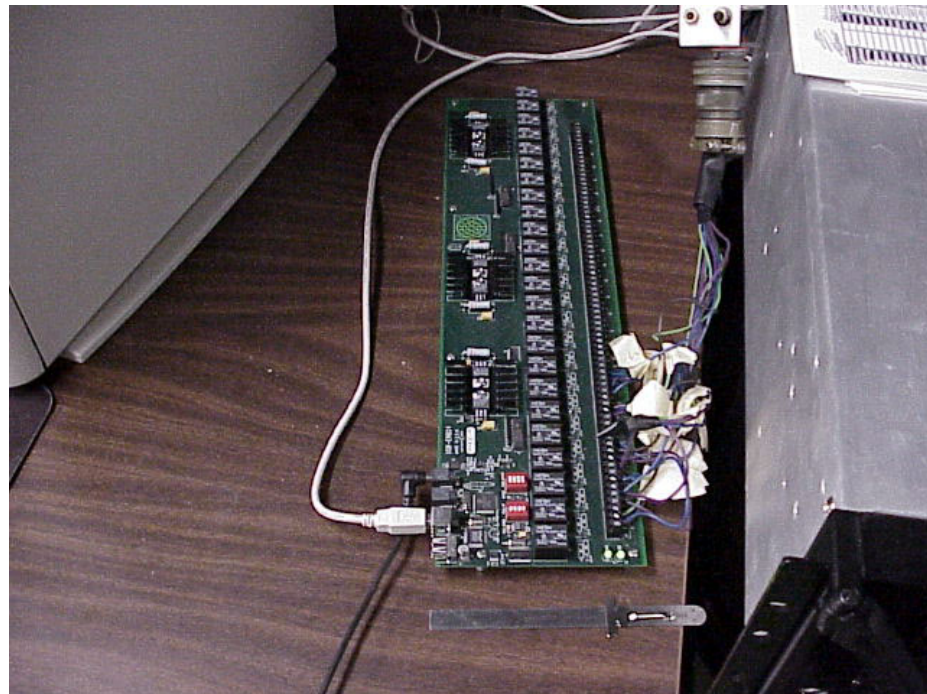


Figure 10. USB ERB-24 remote relay controller

It was addressed by the PC using a USB 2.0 connection. The USB ERB-24 was an electromechanical relay with 24 single-pole, double-throw relays, configured in two banks of eight and two banks of four relays. Each relay had a minimum closed time of 10 milliseconds and a minimum open time of 5 milliseconds. (Measurement Computing “USB ERB-24”, 2005) The controller was called and activated using a MATLAB driver written by Villescas. (Villescas, 2005)

E. PMD-1608FS ANALOG AND DIGITAL I/O MODULE

The PMD-1608FS, pictured in Figure 11, is an eight channel USB analog to digital converter which was used to translate the pressure transducer and probe actuator

signals into digital data in a PC via a USB interface. (Measurement Computing “PMD-1608FS”, 2005)



Figure 11. PMD-1608FS analog and digital I/O module

Two PMD-1608FS modules were called and controlled via a MATLAB control command, different than the USB-ERB24. (Villegas, 2005) One module relayed the data from the two motors on the probe actuator as well as the five pressure transducers connected to the five pressure ports of the five-hole probe. The second module relayed the data from the pressure transducers connected to the stagnation and static probes. A wiring schematic is shown in Figure 12.

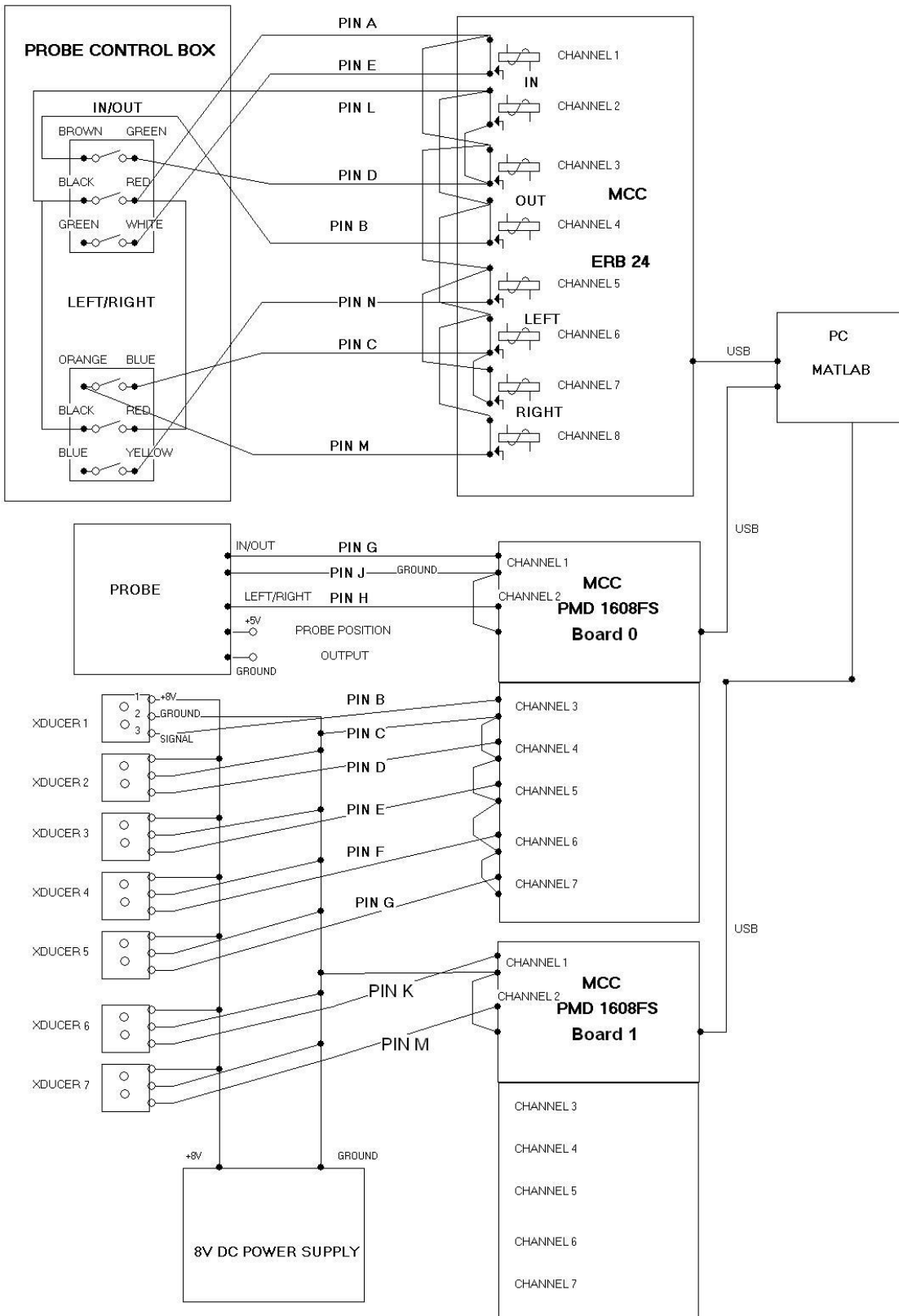


Figure 12. Wiring diagram for probe transducer acquisition

F. MATLAB 6.5 R13

MATLAB version 6.5, release 13 was used as the primary programming compiler for the programs used in the calibration and application of the five-hole probe. The data acquisition programs and graphical user interface were created by Villescas; however minor alterations were made to accommodate the second PMD-1608FS module as well as the two additional pressure transducers. The programming is explained in detail by Villescas. (Villescas, 2005) Changes were made to the PMD_1608FS_3.m, pressure_calibration.m, and OUTPUT_TO_EXCEL.m source files. The PMD_1608FS_3.m source file was altered and split into two files, PMD_1608FS_3_1.m and PMD_1608FS_3_2.m, in order to access pressure transducer data from the first and second PMD-1608FS module, respectively. Source codes are given in Appendix C-1 and C-2, respectively. The pressure_calibration.m source file was altered and split in the same manner and saved as pressure_calibration_1.m and pressure_calibration_2.m; the source codes are given in Appendix C-3 and C-4, respectively. These two programs were used to convert the voltage data obtained from the pressure transducers into usable pressure readings. Finally, OUTPUT_TO_EXCEL.m was modified to accept the previously mentioned, altered source files; this source code is given in Appendix C-5. These changes allowed the original programs created by Villescas to take readings for all seven pressure transducers as well as the two controls for the USB ERB-24 control of the probe actuator and to export the data into an Excel spreadsheet for post-processing.

THIS PAGE INTENTIONALLY LEFT BLANK

IV. FREE-JET CALIBRATION

A. PURPOSE

The purpose of calibrating a multi-hole pressure probe in a known flow was that when it was used in an unknown flow-field its five pressures could be used to derive flow angle and Mach number. For the five-hole probe this was done by first finding the balancing point of the probe in the yaw direction, i.e. equalizing the pressures in ports 2 and 3 as shown in Figure 7. From the values of the pressures at zero yaw and known pitch rotations, a Mach number was obtained from the measured pressure data from the reference probes at the balanced point. (Anderson, Olson, Shreeve, 1977)

B. PROCEDURE

The procedure for calibrating the five-hole probe was similar to the process described by Villescas for a three-hole probe. The only major difference was the adjustment of the pitch of the probe. The process of calibrating the probe began by first calibrating the pressure transducers. One port of the pressure transducer was connected to a known pressure (regulated from the shop air compressor) and the other port was open to the atmosphere. The atmospheric pressure was obtained from a calibrated barometer and the shop compressor pressures were read from a calibrated gauge. The corresponding outputs of the pressure transducers were recorded through the data system and then corresponded to a known differential pressure. The calibration air pressure was set at pressures, 0 to 16 inches of mercury in 2 inches of mercury increments, and the electrical outputs from the pressure transducers were recorded using the MATLAB programs PMD_1608FS_3_1.m and PMD_1608FS_3_2.m, respectively. The voltages and associated known pressures were then input into the MATLAB source code for pressure_calibration_1.m and pressure_calibration_2.m; which calculated curve fits to the data points.

Once the pressure transducers were calibrated they were reconnected to the five-hole probe. This ensured that the readings from the five-hole probe would be accurate to within 0.5% of the actual value. The probe was then mounted in the L.C. Smith probe actuator and attached to the adjustable pitch mount on the modified top plate of the free-jet rig. The data acquisition system recorded pressure data from each of the seven

pressure ports, five on the probe and one each from the stagnation and static probes, as well as the angle of rotation in the yaw direction. The pitch values were read from a machined scale on the pitch mount. The probe was rotated between -30° and 30° yaw in five degree increments for an array of Mach numbers at a specific pitch angle. The Mach numbers were varied by adjusting the dump valve on the Allis-Chalmers compressor to produce flow Mach numbers of 0.3, 0.5, 0.7, and 0.85. Next the flow was slowed to a Mach number of 0.3 and a manual shut-off valve was closed enough to slow the flow to Mach numbers of 0.22 and 0.15. Calibration data were obtained at pitch angles of 0°, 10°, 30°, -5°, -10°, -20°, and -30° at each Mach number.

C. DATA COLLECTION

The data were collected using the MATLAB programs and graphical user interface created by Villescas for the three-hole probe, but modified to record data from the additional pressure transducers. The master program controlled by the graphical user interface required input for the limits of rotation as well as the number of points. These values were -30° to 30° with 13 points, which caused the program to make 13 stops in its rotation from -30° to 30°, or one stop every 5°. Another required parameter was the temperature recorded by a thermocouple connected to a different data acquisition system. (Villescas, 2005)

Once all of these values were input into the program, the actuator proceeded to rotate the probe to each desired yaw angle under programmed control. At each yaw angle, the probe's angular position was recorded based on the feedback from the actuator motors through the USB ERB-24, and the calibration source files for the rotation of the probe. Along with the angle data, the pressure transducers relayed voltages through the PMD_1608FS_3_1.m and PMD_1608FS_3_2.m functions; which were converted into pressure data by the pressure_calibration_1.m and pressure_calibration_2.m functions, using the curves fit to the calibration data for each pressure transducer. Finally all of the calculated parameter values were exported to an Excel spreadsheet.

D. CALIBRATION EQUATIONS

In the Excel spreadsheet the raw data were then reduced into usable pressure coefficients. The calibration nomenclature is given in table 1.

Variable	Parameter
β	Yaw Coefficient
γ	Pitch Coefficient
P_1	Pressure from Pressure Port #1
P_2	Pressure from Pressure Port #2
P_3	Pressure from Pressure Port #3
P_4	Pressure from Pressure Port #4
P_5	Pressure from Pressure Port #5
P_{23}	Average of Side Port Pressures

Table 1. Calibration nomenclature

The yaw coefficient, β , and the pitch coefficient, γ , were calculated with known yaw and pitch values for each known Mach number using the following equations.

$$\beta = \frac{P_1 - P_{23}}{P_1} \quad 4.1$$

$$\gamma = \frac{P_4 - P_3}{P_1 - P_{23}} \quad 4.2$$

$$P_{23} = \frac{P_2 + P_3}{2} \quad 4.3$$

The purpose of the calibration was to establish the dependence of β and γ on the Mach number and pitch angle. When the probe was then used to measure the flow in the compressor inlet, the Mach number and pitch angle could then be derived iteratively, from these relations. (Anderson, et. al. 1977) It should be noted that while the probe was calibrated for variation in yaw angle, it was used only in the “yaw balanced” mode, using only the calibration data obtained at zero yaw angle.

E. CALIBRATION RESULTS

The plots of β vs. yaw angle and Mach number, at zero pitch angle, and γ vs. pitch angle and Mach number, at zero yaw angle, are shown in Figures 13 and 14, respectively.

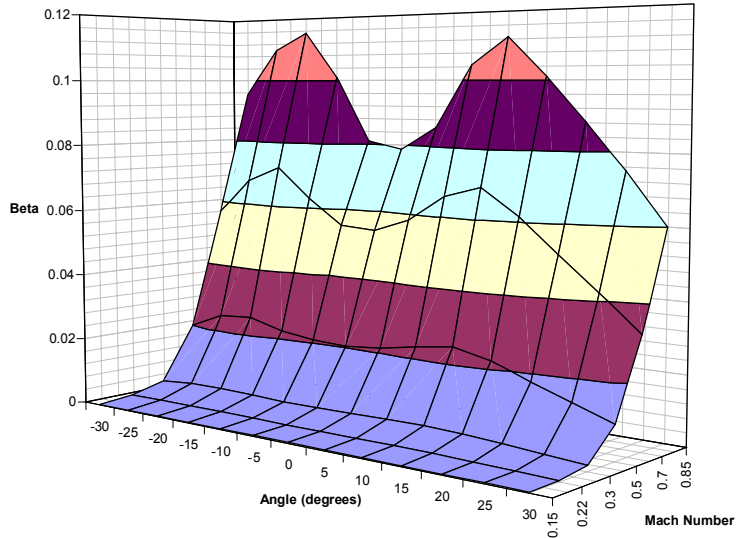


Figure 13. Beta vs. yaw angle and Mach number calibration plot

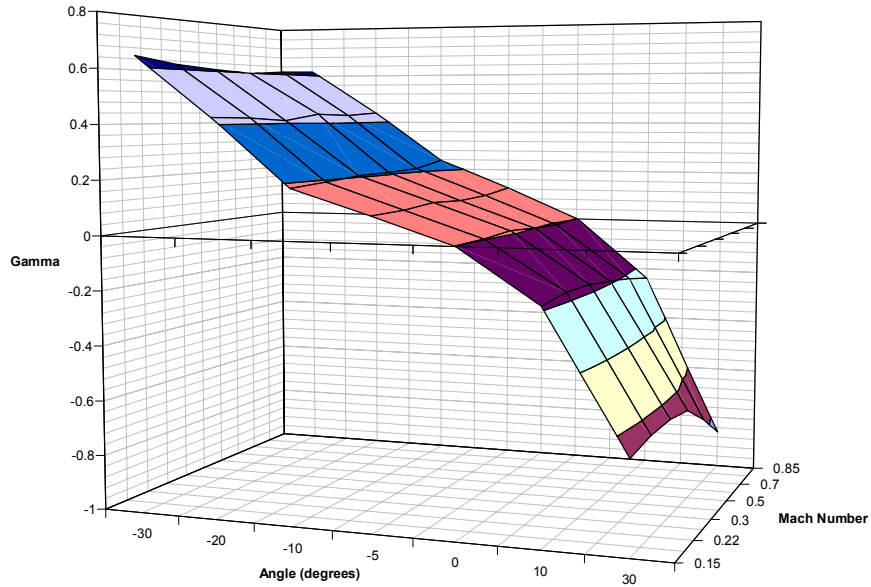


Figure 14. Gamma vs. pitch angle and Mach number calibration plot

Since yaw angle setting and pitch angle setting were fixed in the application of the probe, a calibration curve could be fit between the β values and the Mach numbers for the fixed yaw angle as well as a calibration curve between the γ values and the Mach numbers for each pitch angle. The fixed yaw angle corresponded to the zero flow yaw angle that balanced the probe. Hence, in the application, with measurements of γ and β

obtained at each location, the Mach number was evaluated first from the value of β (at zero pitch). Then the value of pitch angle was obtained iteratively from the expressions for γ as a function of Mach number at each pitch angle. (It was observed in the calibration data that the effect of pitch angle on β was extremely small over the range of pitch angle in the experiment.)

THIS PAGE INTENTIONALLY LEFT BLANK

V. TRANSONIC COMPRESSOR RIG EXPERIMENTATION

A. PROCEDURE

The procedure used for obtaining data in the transonic compressor rig was similar to the upstream test procedure outlined by Villescas. The yaw angle required to balance the probe was approximately -5° of yaw, measured clockwise with respect to the upstream direction. Because the probe and actuator were mounted directly to the case wall of the transonic compressor rig, the pitch angle of the probe was fixed, and zero pitch angle corresponded to flow parallel to the duct wall. Since the pitch angles were expected to be small, the first estimate of the Mach number was obtained by applying the calibration data at a pitch angle of 0° .

After the probe was balanced within the flow, the probe traversed and collected data at 13 specific locations in the flow, extending from the case wall towards the centerline of the flow. The 13 specific points were determined by dividing the distance from the case wall to the centerline of the inlet by a cosine function the same way as the upstream points were determined for the three-hole probe measurements. However, the three-hole probe utilized 15 points instead of 13 points because of its greater over all length. Since the five-hole probe was 3cm shorter than the three-hole probe, the last two locations could not be reached. A table of the sampling positions is shown in table 2. (Villescas, 2005)

Position Number	Radial Depth in cm.
1	10.86
2	9.36
3	7.91
4	6.54
5	5.26
6	4.09
7	3.05
8	2.14
9	1.38
10	0.78
11	0.35
12	0.09
13	0

Table 2. Sampling positions

Data were taken at all 13 distances for the flow conditions corresponding to 30, 40, 50, 60, 70, 80, 90, and 100 percent of the design speed for open throttle conditions. The data are tabulated in Appendix D. The 100 percent speed corresponded to the design speed of 27,085 revolutions per minute. Data were also obtained for peak-efficiency and near-stall conditions for the 70 and 90 percent design speeds. (Villescas, 2005)

B. EXPERIMENTAL RESULTS

Inlet surveys of the Mach number distribution were obtained at each test condition. Plots of the Mach number in relationship to the position from the case wall are shown in Figure 15 for the open throttle conditions for 70, 90 and 100 percent design speed.

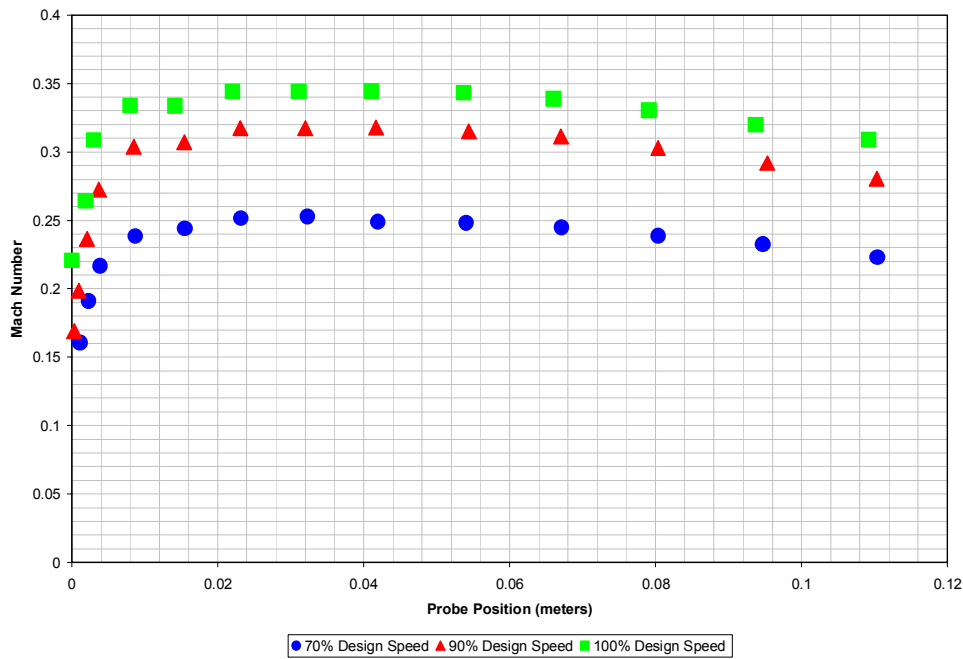


Figure 15. Mach number distribution at open throttle conditions

The maximum Mach number value rose from 0.25 for 70 percent design speed to 0.32 for 90 percent design speed, and finally up to 0.35 for 100 percent design speed. The trends in the boundary layer thickness and the presence of a drop in Mach number approaching the centerline, are similar at all speeds. The boundary layer was about 0.004 meters from the case wall, but all three plots show a small plateau at the edge of the layer. This was thought to be possibly an “immersion effect” of the United Sensor probe at this distance from the wall. (Anderson, et. al. 1977)

Next the results for the 70 percent runs at open-throttle, peak-efficiency, and near-stall were plotted as shown in Figure 16.

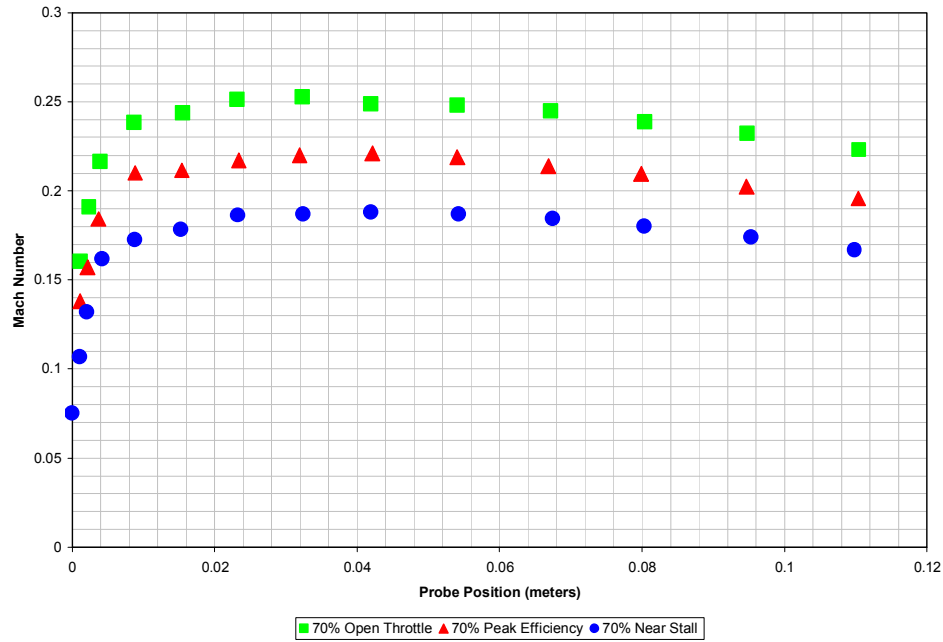


Figure 16. Mach number distribution at 70% design speed conditions

The Mach number for the 70 percent runs increased from 0.18 at the near-stall condition, to 0.22 at the peak-efficiency condition, to a maximum of 0.25 at the open-throttle condition. The plots also showed gradual drops in the Mach number distributions caused by the center body.

Finally, Mach number distributions for the 90 percent conditions were plotted as shown in Figure 17.

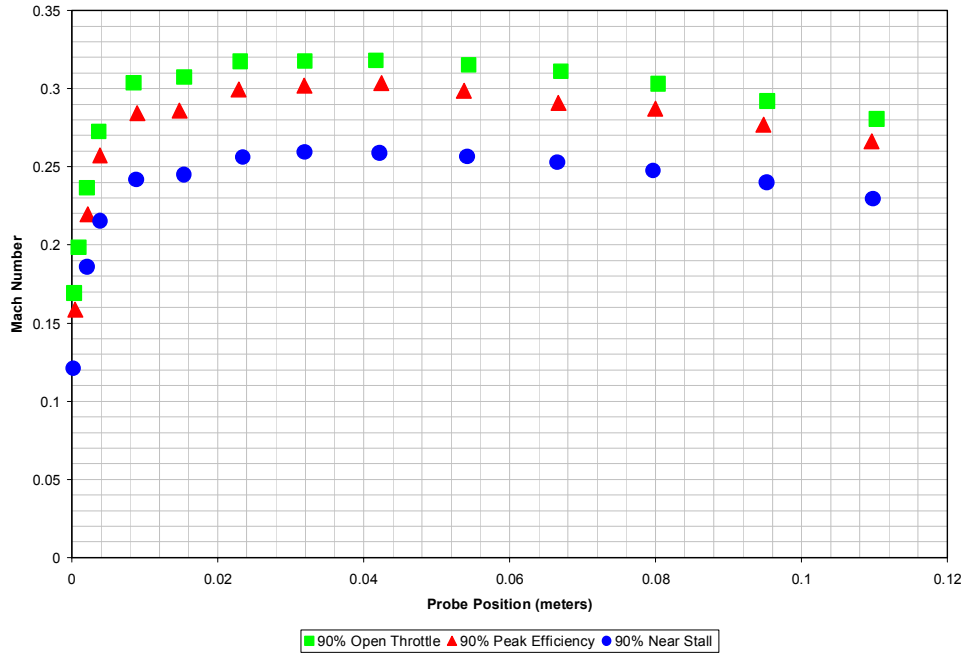


Figure 17. Mach number distribution at 90% design speed conditions

These plots showed the same general trends in boundary layer thickness as well as a drop approaching centerline. However the maximum mach numbers varied from 0.26 at the near-stall condition, to 0.30 at peak-efficiency, all the way up to 0.32 at the open throttle conditions. All of these results were analyzed more in depth in comparison with the CFD results.

In addition to the Mach number distributions, the effective pitch angle of the flow was determined. Figure 18 shows the angle of pitch in the flow for each probe position for the 90 percent design speed conditions.

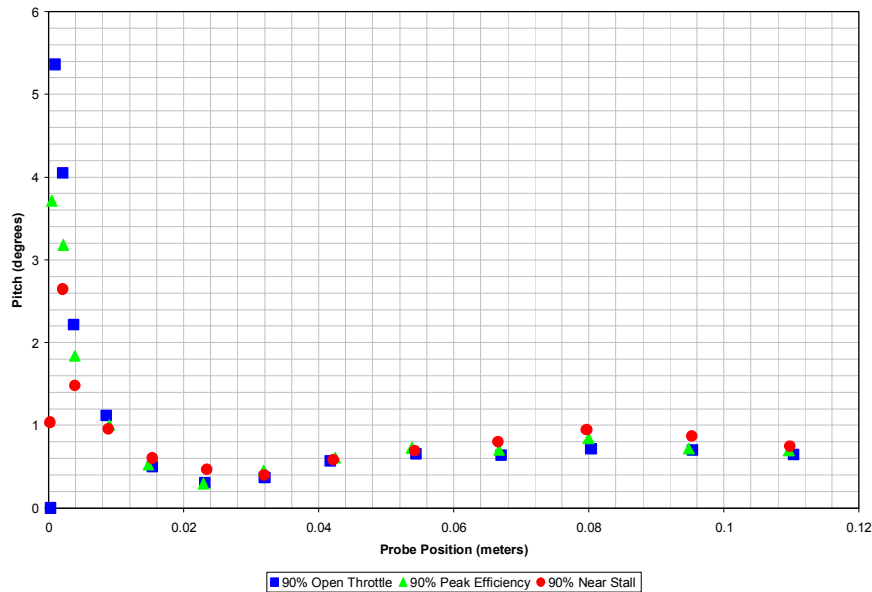


Figure 18. Magnitude of the flow pitch towards the centerline

The magnitude of the flow pitch angle was indicated to rise inside of the boundary layer to as high as 6° of pitch, and quickly decrease to approximately 0.5° outside of the layer. The pitch angle then rose to approximately 1° as the flow adjusted to move around the center body. This showed that the flow had an off-axis velocity component due to the disturbance caused approaching the spinner. It is noted that the distribution of pitch angle derived from the measured data, using curve fits to calibration data and an iterative procedure, were extremely smooth. It is also noted, however, that the overall uncertainty in the method is estimated to be about 0.5° in the pitch angle, so that the minimum pitch angle in the flow may have been zero.

THIS PAGE INTENTIONALLY LEFT BLANK

VI. CFD MODELLING

A. DESCRIPTION OF CODES

Two specific CFD program suites were utilized in calculating analytical results. Both were marketed by Ansys Inc. and both were chosen because of specific desirable attributes.

1. ICEM CFD

ICEM CFD (Ansys, 2005) was the primary program used in creating the computer aided drawings and structured meshes. It was chosen because of its ability to develop structured, unstructured, and hybrid meshes for specific models as well as its automatic mesh generation tools. The meshes created by ICEM CFD were also compatible with the CFX-5 solver.

2. CFX-5

CFX-5 (Ansys, 2005) was the primary program suite used in the assignment of boundary conditions, solving the equations of motion on the mesh and analyzing the calculated results. The CFX-5 suite was divided into three specific interfaces; Pre, Solver, and Post. The Pre component of the CFX-5 suite was used to assign boundary conditions to the mesh generated by ICEM CFD. One of the most important aspects of Pre was the ability to model multiphase flow as well as an extensive and complex library of materials including water vapor or steam.

Solver was the actual computational solver of the CFX-5 suite which integrated the Navier-Stokes equations using a coupled multi-grid algebraic solver. Another key aspect of Solver was the ability to run a single computation in parallel on multiple computer systems over a network. This allowed for shared processing and faster calculations.

Post was the post-processing module in the CFX-5 suite. This particular program was used to extract specific information from the calculated results.

B. CFD MODELS

1. Air Inlet Duct

The model for the air inlet duct is displayed below in Figure 19.

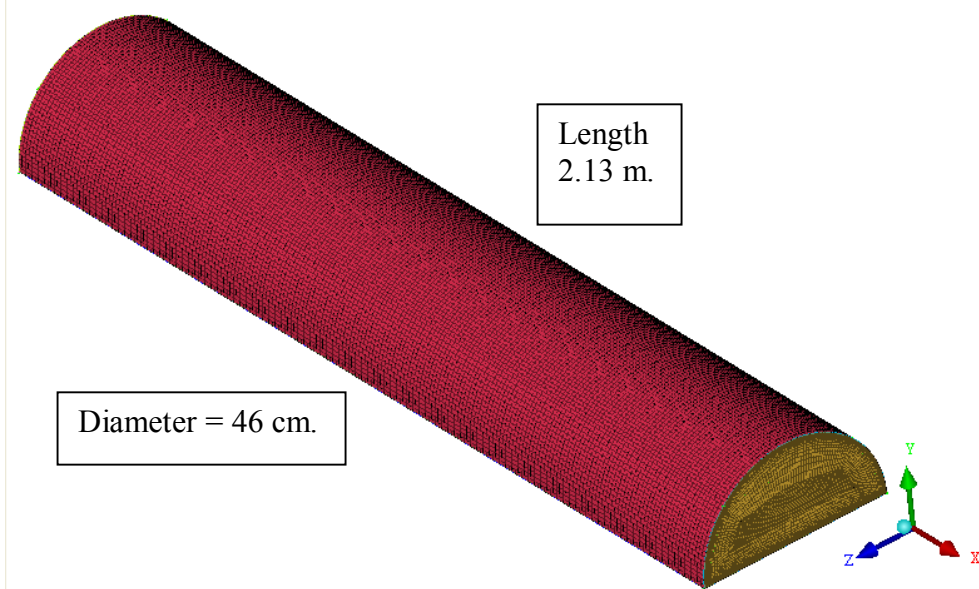


Figure 19. Air inlet duct CFD model

This model was based on the dimensions of the duct connected to the inlet of the transonic compressor rig. This particular model consisted of an inlet, outlet, wall, and symmetry condition along the center plane of the duct. The mesh consisted of 870,476 total elements within a single volume block with O-grids at the inlet and outlet of the duct. The mesh at the inlet and outlet were spaced as an exponential function towards the duct wall. This was important in order to calculate results closer to the duct wall, to analyze boundary layer development.

2. Inlet Distortion Duct

The model for the inlet distortion duct is displayed below in Figure 20.

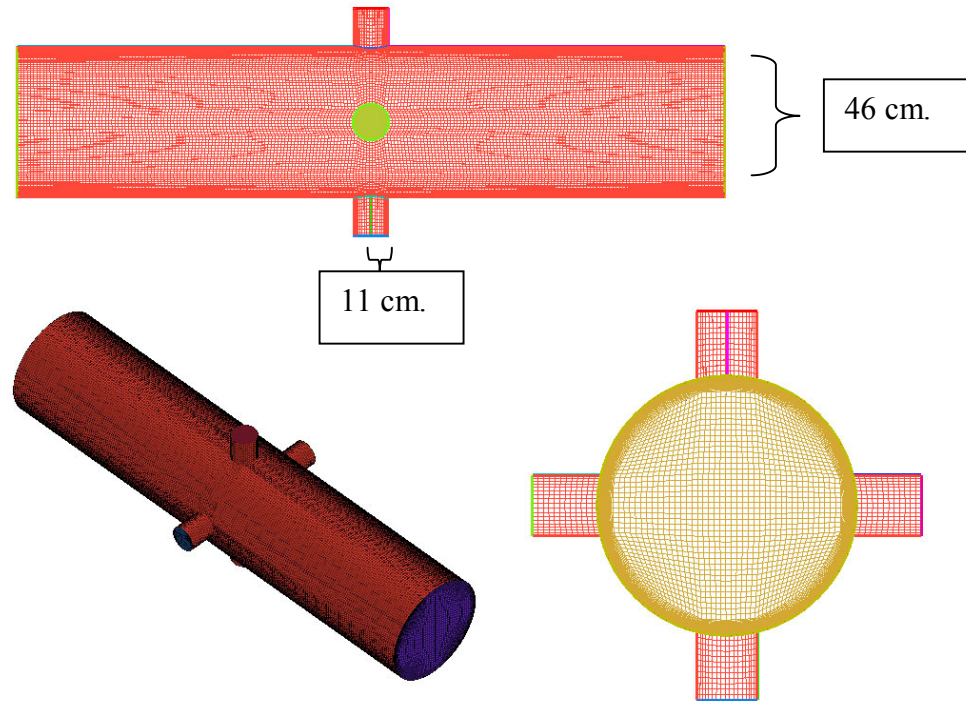


Figure 20. Inlet distortion duct CFD model

This model was created with the same dimensions as the inlet distortion duct design, the design of which is displayed in Appendix E. This particular model consisted of an air inlet, outlet, wall, and four individual flow injectors spaced equally around the diameter of the duct. The mesh consisted of 1,317,607 total elements with O-grids at the inlet, outlet and at each of the injectors and a structured H-grid mesh along the surface.

3. Inlet Bell-Mouth

The model for the inlet bell-mouth is displayed below in Figure 21.

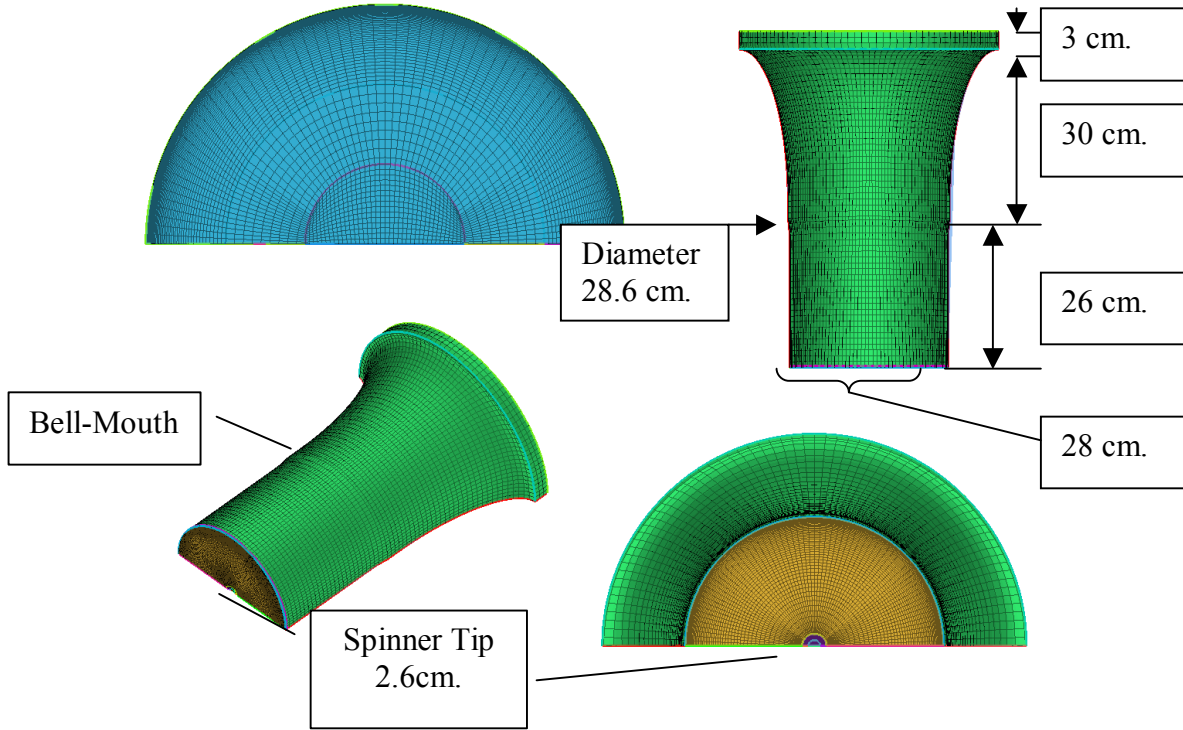


Figure 21. Inlet bell-mouth grid

This model was created with the measured dimensions of the inlet bell-mouth of the Transonic Compressor Rig. This particular model consisted of an inlet, outlet, wall, a symmetry condition along the center plane of the model, a small section of the rotor spinner tip obstructing part of the outlet. In addition, the model included a distortion along the surface where the two sections of the bell-mouth interfaced. The mesh consisted of 298,762 total elements with two concentric O-grids at the inlet and outlet and a structured H-grid along the wall, hub tip, and symmetry plane.

C. CFD MACH NUMBER CALCULATION RESULTS

Calculations were made of the flow through the inlet bell-mouth using boundary conditions based on the pressure data from the stagnation and static pressure probes in the transonic compressor rig. A survey of the Mach number distribution was taken at the same distance from the rotor hub as the five-hole probe. These surveys were taken for 70, 90, and 100 percent open throttle conditions as well as peak-efficiency and near-stall

conditions for 70 and 90 percent design speed. The stagnation and static pressures, used in calculating the boundary conditions for the CFD modeling, are given located in table 3.

Open-Throttle Conditions		
% Design Speed	Ps	P0
70	92854.59	97034.61
90	88463.04	95223.32
100	108253.88	116042.68
Peak-Efficiency Conditions		
% Design Speed	Ps	P0
70	86798.14	89804.99
90	77894.43	83300.38
Near-Stall Conditions		
% Design Speed	Ps	P0
70	83651.43	85754.55
90	72792.58	76329.23

Table 3. Boundary conditions used in each CFD model

These pressure values correspond to the average inlet stagnation pressures and exit static pressures recorded by the stationary probes over the duration of the probe traverse.

THIS PAGE INTENTIONALLY LEFT BLANK

VII. COMPARISON OF RESULTS

Before the CFD results were compared to the five-hole probe data, the five-hole results were first compared with the results from the three-hole probe experiments. The results are given in Figure 22.

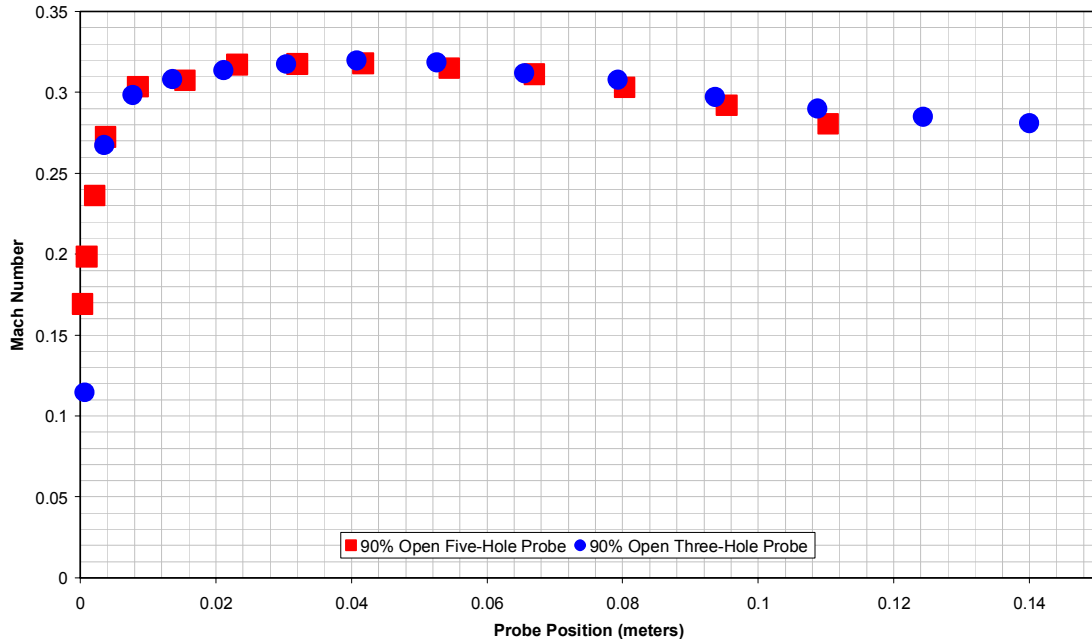


Figure 22. Comparison of five-hole and three-hole probe data

In comparing these two sets of data, the five-hole probe showed very similar trends, with very minute differences in the Mach numbers approaching the centerline as well as in the shape of the boundary layer. The close agreement in the two sets of independent probe data, suggested that both the five-hole probe and the three-hole gave acceptable measures of the flow field.

Next, a plot of the Mach number distribution at open throttle conditions for 70, 90, and 100 percent design speed obtained from the experimental probe data and from the

CFD results is shown in Figure 23. The 70, 90 and 100 percent speed conditions were chosen because they were the most frequently set operational speeds of the transonic compressor.

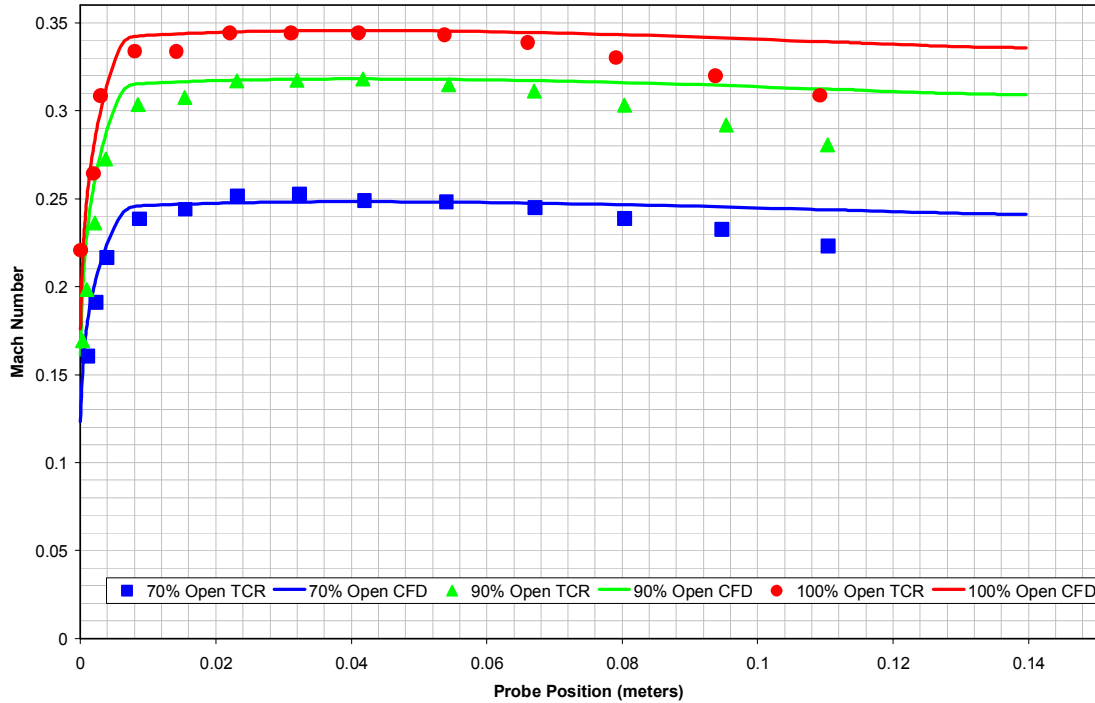


Figure 23. Open-throttle Mach number distribution comparison

The general trend and values of both the CFD and experimental results were in agreement. First, the thickness of the boundary layer was similar, around 0.004 meters from the case-wall. The experimental result, however, showed a small plateau near the edge of the boundary layer. This was possibly due to the “immersion effect”. (Anderson, et. al. 1977) This plateau was not apparent in the three-hole probe results because of the design differences in the probes. The three-hole probe was constructed with the pressure ports at the end of the probe and slightly forward of the shaft; however the five-hole probe had the ports approximately one centimeter from the tip of the probe, and on the shaft. The three-hole probe would be less influenced by the wall when measuring close to the wall. However, the Mach number values recorded away from the wall were nearly identical between the two methods and differed by only 2% of the experimental values. Finally the trends of the experimental and CFD results were

comparable. Both sets of data showed a steady flow at the maximum value and then a gradual drop in Mach number toward the centerline, caused by flow interaction with the center body. The difference in the extent of the drop off could be attributed to the specific CFD model, since only a small section of the spinner was included in the computation.

A comparison of the Mach number distributions for the open throttle, peak-efficiency, and near-stall conditions for 70 percent design speed from the experimental probe data and the CFD results is shown in Figure 24.

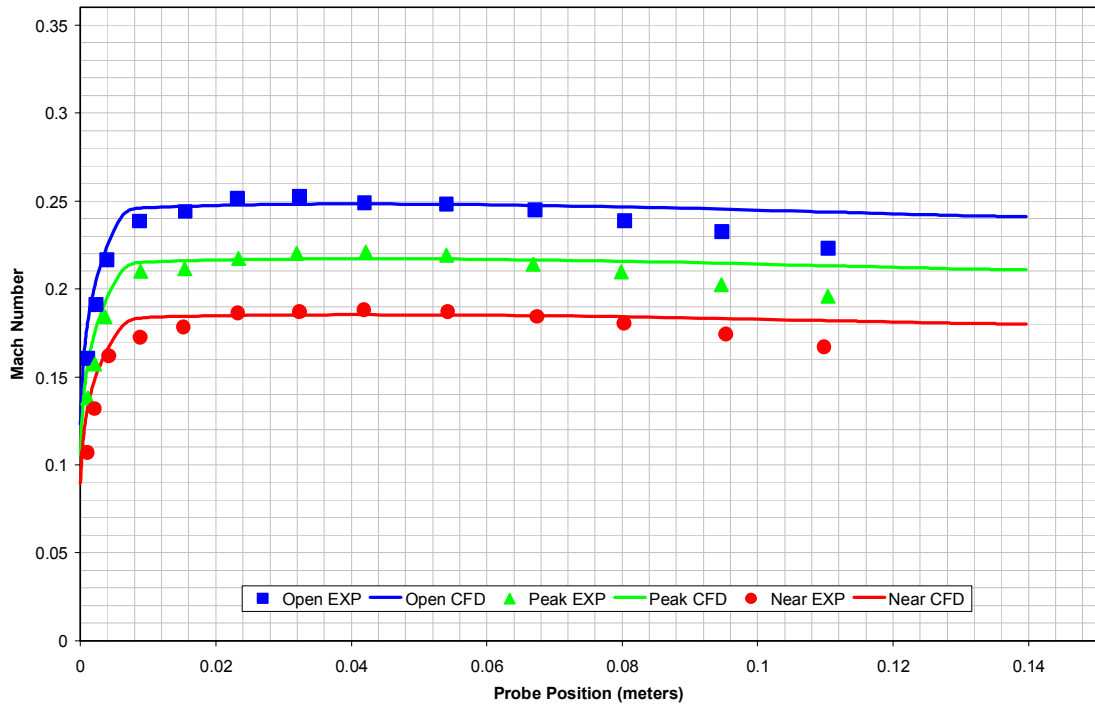


Figure 24. 70% design speed Mach number distribution comparison

The results from the 70% design speed showed the same trends as were previously mentioned. The most noticeable difference is the extent of the plateau at the edge of the boundary layer as well as the difference in the drop in Mach number towards the centerline. Because of the lower flow velocity, these differences were not as noticeable as in the higher speed flows.

Finally, a plot of the 90 percent design speed results is shown in Figure 25.

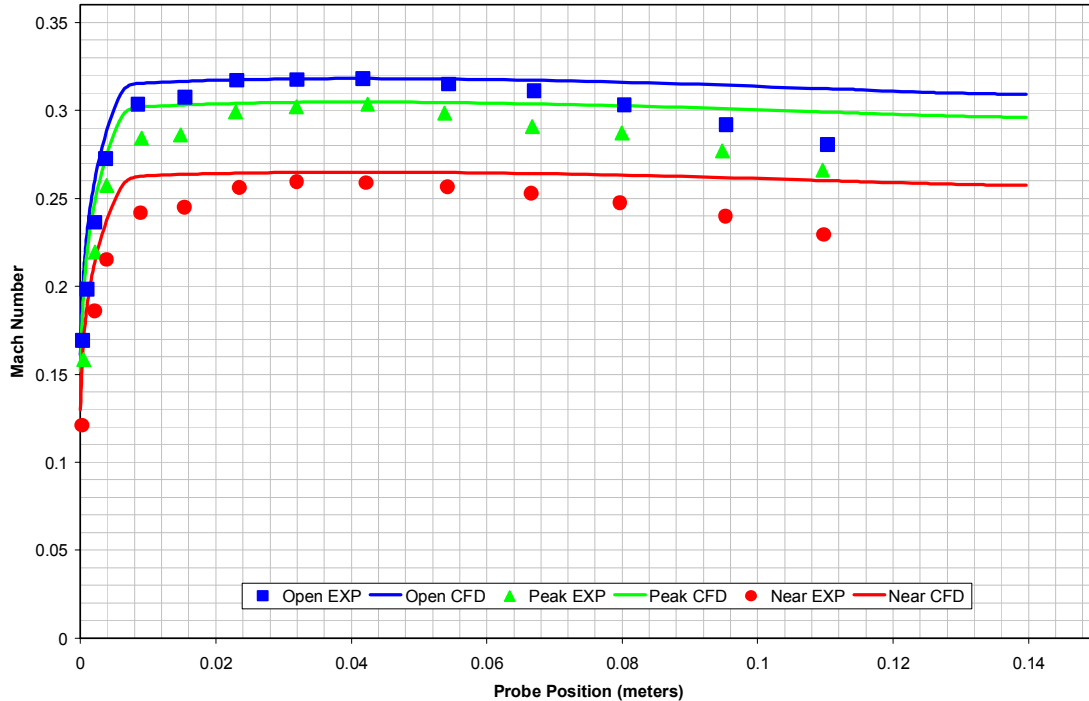


Figure 25. 90% design speed Mach number distribution comparison

The 90 percent speed results showed larger differences between the experimental and CFD results. This was especially apparent in the boundary layer thickness. The results from the peak-efficiency and near-stall conditions showed as much as 9% difference between the experimental and CFD results near the edge of the boundary layer. However, all throttle conditions showed good agreement outside of the layer, and differed towards the centerline by less than 13%. With more detailed CFD modeling these differences will be reduced.

Finally, in order to facilitate future use of the CFD modeling, a brief demonstration of multiphase steam/air flow was performed using the models. The computation used random conditions and was done to demonstrate the ability to mix fluids in the CFD code. An explanation of the boundary conditions as well as an explanation of the process are given in Appendix F.

VIII. CONCLUSION

The present study succeeded in expanding on previous probe surveys and set up the CFD models to use in future calculations of the global flow-field. While multiphase flow was eventually modeled, a lack of actual operating conditions for the steam injection limited the applicability of the actual multiphase results in the current study. However, the ability and steps to perform multiphase flow were demonstrated in providing the groundwork for future CFD modeling.

The five-hole probe measurements matched the results from the three-hole probe, with very small differences. The five-hole probe proved useful in determining the pitch angle of the flow, particularly close to the centerline where the effect of the spinner was evident.

The computational results agreed reasonably well with the experimental results; however a complete model of the transonic compressor, including the full rotor hub is required to decrease the departure from the experimental data. The CFD code also does a very good job of approximating the upstream conditions of the flow and developing a realistic boundary layer.

THIS PAGE INTENTIONALLY LEFT BLANK

IX. RECOMMENDATIONS

In future studies, the five-hole probe will be needed to measure the flow into the compressor stage. Because of the contraction over the spinner, the flow is not axial and pitch measurements are required. Also, when steam is injected into the upstream flow, the mixing of the fluids will cause non-axisymmetric changes in the direction of the inlet flow.

The CFD models need to be combined in order to fully calculate the flow through the complete inlet ducting. This complete model would encompass the air inlet duct model, the inlet distortion duct, the inlet bell-mouth, and finally a turbo model of the rotor hub and Sanger rotor. Also, experimental data are needed for the boundary conditions to be used with steam injection to fully simulate the multiphase flow through the compressor. Once these values are obtained and modeled in the full CFD model, an analytical prediction of the effects of steam ingestion through a transonic compressor can be obtained.

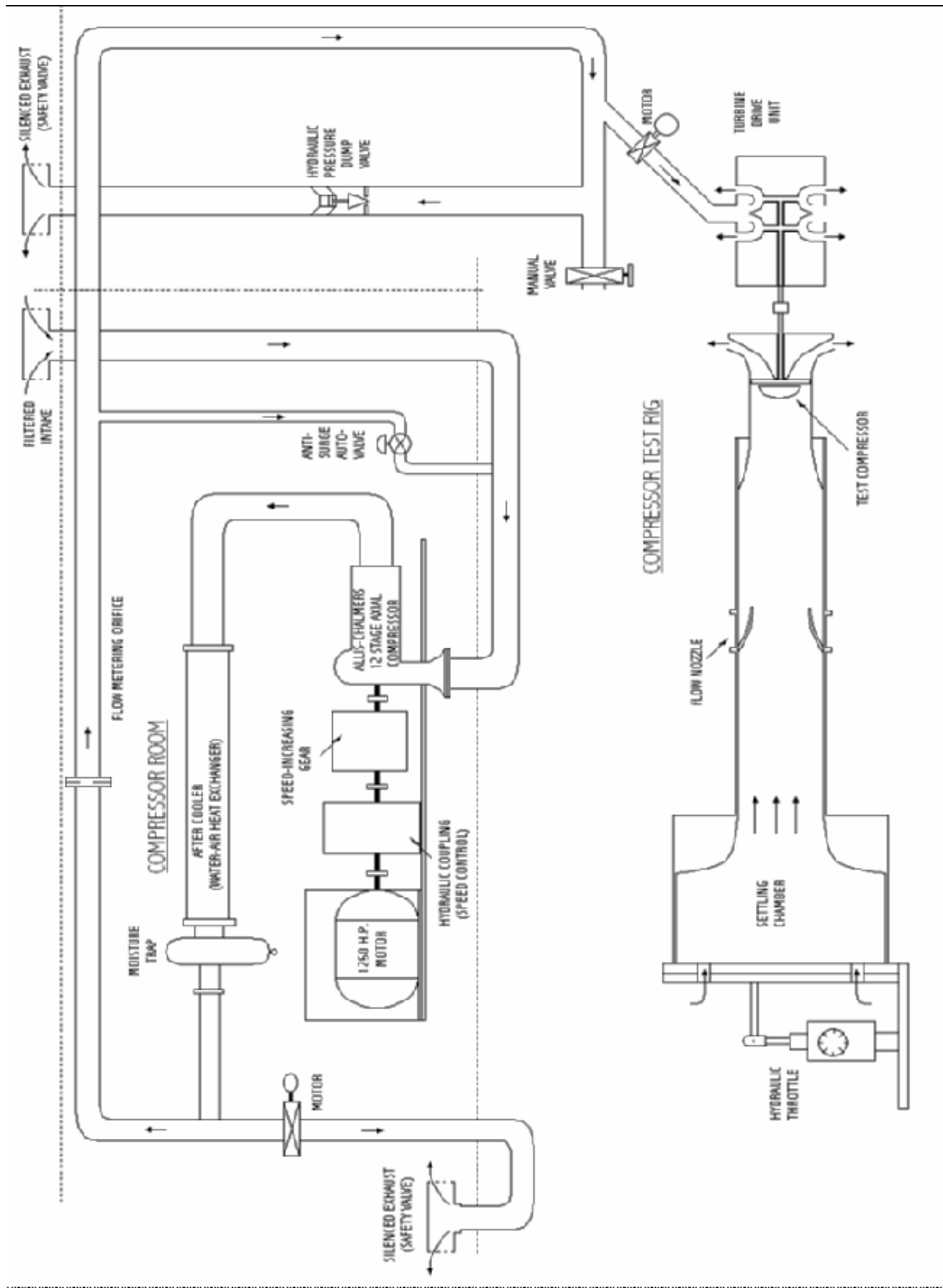
THIS PAGE INTENTIONALLY LEFT BLANK

LIST OF REFERENCES

1. Anderson, D.J., Olsen, J.A., Shreeve, R.P., 1977, "Velocity Vector Determination from Multiple-Sensor Pneumatic Probe Measurements," AIAA 1977, 9th Fluid and Plasma Dynamics Conference, San Diego California
2. ANSYS Inc., "ANSYS ICEM CFD," Product Details, ansys.com, 2005
3. ANSYS Inc., "ANSYS CFX," Product Details, ansys.com, 2005
4. Donelson, S. Briggs, T., *"JSF Team Probes Steam Catapult Environment,"* JSF Integrated Test Force, dcmilitary.com, February 6, 2003.
5. Gannon, A.J., Hobson, G.V., Shreeve, R.P., "Measurement of the Unsteady Casewall Pressures Over the Rotor of a Transonic Fan and Comparison with Numerical Predictions", ISABE 2005, 17th International Symposium on Airbreathing Engines, Munich, September 2005.
6. Measurement Computing, PMD-1608FS USB Based Analog and Digital I/O Module User's Guide. May 6, 2005.
7. Measurement Computing, USB-ERB24 USB Based 24 Relay Module User's Guide. May 4, 2005.
8. O'Brien, J.M., "Transonic Compressor Test Rig Rebuild and Initial Results with the Sanger Stage", Master's Thesis, Naval Postgraduate School, Monterey, California, June 2000.
9. Omega.com, "Low Cost Silicon Pressure Sensor, PX 138 Series", 2005 Stamford Connecticut.
10. Sanger, N. L., "Design of a Low Aspect Ratio Transonic Compressor Stage Using CFD Techniques," ASME Journal of Turbomachinery, July 1996, Vol. 118 pp 479-491.
11. Sanger, N. L., *"Design Methodology for the NPS Transonic Compressor,"* TPL Technical Note 99-01, August 1999.
12. Villescas, I., "Flow-field Surveys in a Transonic Compressor Prior to Inlet Steam Ingestion Tests", Master's Thesis, Naval Postgraduate School, Monterey, California, September 2005.

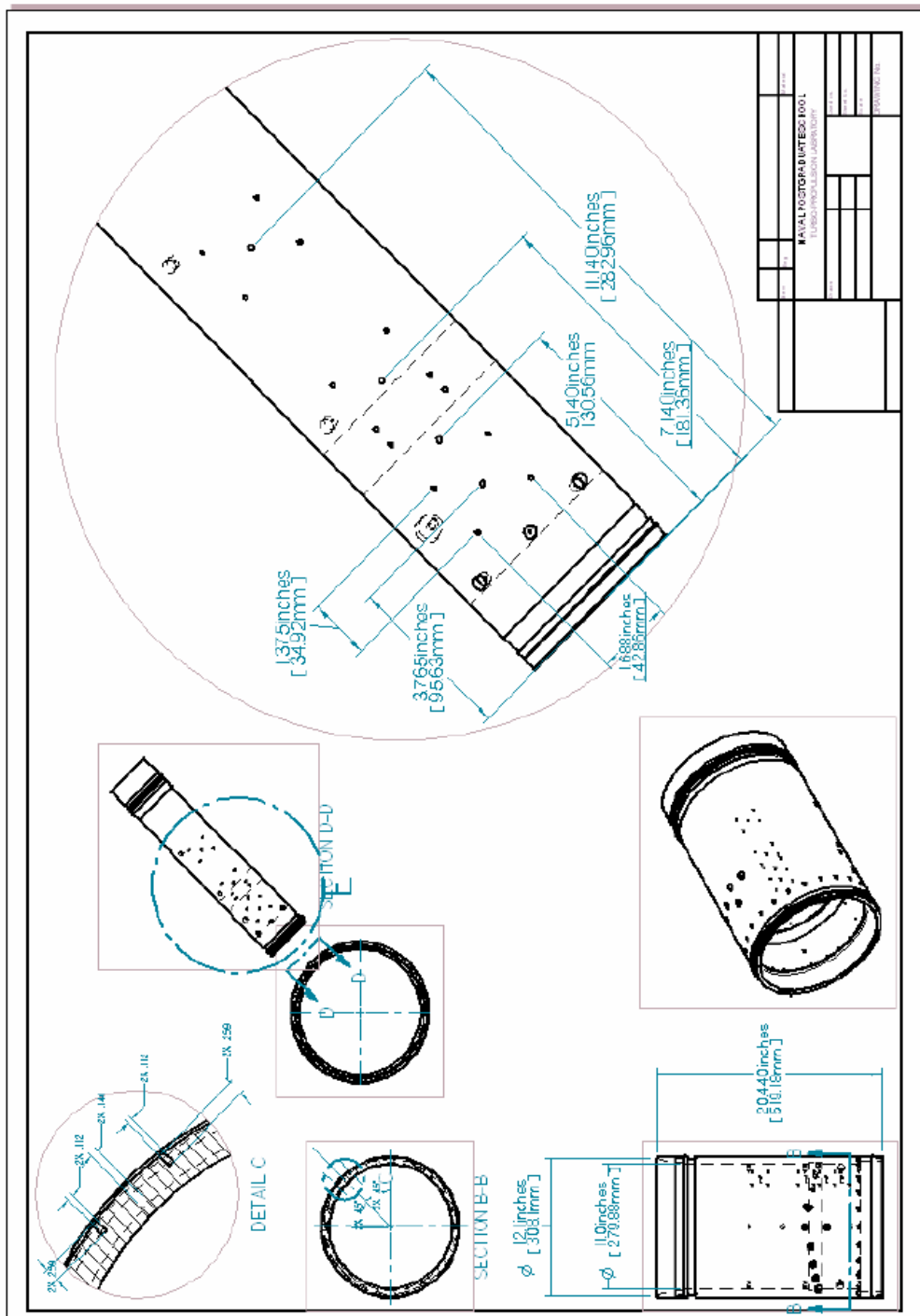
THIS PAGE INTENTIONALLY LEFT BLANK

APPENDIX A – TRANSONIC COMPRESSOR RIG SETUP



THIS PAGE INTENTIONALLY LEFT BLANK

APPENDIX B – CASE WALL SCHEMATIC



THIS PAGE INTENTIONALLY LEFT BLANK

APPENDIX C – MATLAB SOURCE CODE

APPENDIX C-1 - PMD_1608FS_3_1.M

```
function[analog_pressure_1]=PMD_1608FS_3_1
%This function is called to take an average the readings of all pressure.
%It will be used for feedback on the pressure of the five hole probe as
%well as static and stagnation pressure.

clear all

global analog_pressure_1


openDAQ=daqfind;
for i=1:length(openDAQ),
    stop(openDAQ(i));
end

%stop(ai);
%delete(ai);
%clear all
ai = analoginput('mcc',0);
%create channel 1-7 (called 0-6)
%1-5 will be the five hole probe, 6,7 will be Po and P1
addchannel(ai,2:6);

set(ai,'SampleRate',500);
ActualAIRate = ai.SampleRate;
set(ai,'SamplesPerTrigger',30)

start(ai)

[a,t] = getdata(ai);

analog_pressure_1=sum(a)/30;

stop(ai);
delete(ai);
```

APPENDIX C-2 - PMD_1608FS_3_2.M

```
function[analog_pressure_2]=PMD_1608FS_3_2
%This function is called to take an average the readings of all pressure.
%It will be used for feedback on the pressure of the five hole probe as
%well as static and stagnation pressure.
```

```
clear all
```

```
global analog_pressure_2
```

```
openDAQ=daqfind;
for i=1:length(openDAQ),
    stop(openDAQ(i));
end
```

```
%stop(ai);
%delete(ai);
%clear all
ai = analoginput('mcc',1);
%create channel 1-7 (called 0-6)
%1-5 will be the five hole probe, 6,7 will be Po and P1
addchannel(ai,0:1);
```

```
set(ai,'SampleRate',500);
ActualAIRate = ai.SampleRate;
set(ai,'SamplesPerTrigger',30)
```

```
start(ai)
```

```
[a,t] = getdata(ai);
```

```
analog_pressure_2=sum(a)/30;
```

```
stop(ai);
delete(ai);
```

APPENDIX C-3 - PRESSURE_CALIBRATION_1.M

```
function[Pressures_1] = pressure_calibration_1

%insert data into x and y to get the calibration curve for rotation.
%the x data used for the angle was taken from digital inclinometer
%the y data was read from the digital pmd1608fs_2

% First calibration.
%(5/3/05)
%pressure in inches of mercury converted to Pascals

global Pressures_1
global analog_pressure_1

analog_pressure_1=PMD_1608FS_3_1;

x=[0 2 4 6 8 10 12 14 16]*3386.39+[29.88]*3386.39;

%Values for Upper pressure connection 5_5_05

y(:,1)=[3.4991
3.3354
3.1726
3.009
2.8524
2.6837
2.5235
2.3596
2.3608
];

y(:,2)=[3.5043
3.338
3.1724
3.0067
2.848
2.6771
2.5142
2.3481
2.349
];

y(:,3)=[3.5004
3.338
3.176
```

```

3.014
2.8585
2.6914
2.5321
2.3699
2.3708
];

y(:,4)=[3.4982
3.3343
3.1716
3.0084
2.8513
2.6825
2.5222
2.3584
2.3595
];
y(:,5)=[3.5075
3.3412
3.1763
3.0105
2.8523
2.6811
2.5185
2.3528
2.3539
];
%y=flipud(y)

for ii=1:5

%create a square polynomial to fit the data to. Data was nearly linear.
p(ii,:)=polyfit(y(:,ii),x,1);

%evaluate the polynomial at the analog position and output the position in
%degrees

Pressures_1(ii)=polyval(p(ii,:),analog_pressure_1(ii));

end

```

APPENDIX C-4 - PRESSURE_CALIBRATION_2.M

```
function[Pressures_2] = pressure_calibration_2

%insert data into x and y to get the calibration curve for rotation.
%the x data used for the angle was taken from digital inclinometer
%the y data was read from the digital pmd1608fs_2

% First calibration.
%(5/3/05)
%pressure in inches of mercury converted to Pascals

global Pressures_2
global analog_pressure_2

analog_pressure_2=PMD_1608FS_3_2;

x=[0 2 4 6 8 10 12 14 16]*3386.39+[29.88]*3386.39;

y(:,1)=[3.4953
3.3305
3.1667
3.0022
2.8439
2.6741
2.5129
2.3494
2.349
];
y(:,2)=[3.4965
3.3323
3.1686
3.0049
2.8465
2.6774
2.516
2.3532
2.3528
];
%y=flipud(y)

for ii=1:2

%create a square polynomial to fit the data to. Data was nearly linear.
```

```
p(ii,:)=polyfit(y(:,ii),x,1);  
%evaluate the polynomial at the analog position and output the position in  
%degrees  
Pressures_2(ii)=polyval(p(ii,:),analog_pressure_2(ii));  
end
```

APPENDIX C-5 - OUTPUT_TO_EXCEL.M

```
function[]=OUTPUT_TO_EXCEL(Tp, Tj)
%this function gets the data from the devices using PMD_1608FS_2 and
%PMD_1608FS_3 and sends the data to ExcelWrite to be written to an Excel
%Spreadsheet.

global Pressures_1
global Pressures_2

%Freddy.txt is a notepad value used to hold on to data outside of the
%program to ensure headers will be created.
load freddy.txt

%restart.txt is a notepad value used to hold on to data outside of the
%program to ensure data will not be overwritten if the run is restarted.
load restart.txt

%if it is the first run, or the run has been restarted, this loop will
%place the header in and then write the first line of data.
if freddy==1;

    %if first line, put the header in. if restart, add the number of
    %lines so that data will not be overwritten.
    a=freddy+restart;

    %header
    m={'angle', 'P1', 'P2', 'P3', 'P4', 'P5', 'Psj', 'P0j', 'Tp', 'Tj', 'q_probe', 'V_jet',
    'Cp1_Probe',...
                    'Cp2_Probe',    'Cp3_Probe',    'At_Probe',    'As_Probe',
    'Mach_No'};

    %create a variable that can be evaluated so that the values of lines
    %can be changed.
    fred = ['ExcelWrite(' " 'C:\Documents and Settings\user\Desktop\Five
    Hole Probe\Calibration\testing1.xls'" ', 0',...
    "' [ num2str(a )' num2str(2) ]'" ', m')'];

    %evaluate the variable and send the info to ExcelWrite to evaluate it and
    %send it to an EXCEL Spreadsheet.
```

```
eval(fred);
```

```
%change the row number it will be the next available.
```

```
%Call the calculation function  
calculate(Tp, Tj);
```

```
%create a variable that can be evaluated so that the values of lines  
%can be changed.
```

```
%fred = ['ExcelWrite(' "'' 'C:\Documents and  
Settings\user\Desktop\ERB24\testing1.xls' ''', 0,'...  
% "' num2str(a) ',' num2str(2) ']' ''', m)];
```

```
%evaluate the variable and send the info to ExcelWrite to evaluate it and  
%send it to an EXCEL Spreadsheet.
```

```
%eval(fred);
```

```
%Change the value of freddy to the next row number.
```

```
%freddy=freddy+1;
```

```
%Save the row number to a text file so that it will not be cleared.  
%save freddy.txt freddy -ascii
```

```
%If the run is not the first, or a reset, just output dats.  
elseif freddy ~=1
```

```
a=freddy+restart;
```

```
%Call the calculation function  
calculate(Tp, Tj);
```

```
%create a variable that can be evaluated so that the values of lines  
%can be changed.
```

```
%fred = ['ExcelWrite(' "'' 'C:\Documents and
```

```
Settings\user\Desktop\ERB24\testing1.xls' ''', 0,'...  
% "' num2str(a) ',' num2str(2) ']' ''', m)];
```

```
%eval(fred);
```

```
%evaluate the variable and send the info to ExcelWrite to evaluate it and  
%send it to an EXCEL Spreadsheet.
```

```
%eval(fred);
```



```
%get the pressure variable info.
```

```
Pressures_1=pressure_calibration_1;  
Pressures_2=pressure_calibration_2;  
%Pressures=PMD_1608FS_3;
```

```
%%%%%%%%%%%%%%  
%%%%%%%%%%%%%%  
%Cobra Probe pressures  
%%%%%%%%%%%%%%  
%%%%%%%%%%%%%%  
%%%%%%%%%%%%%%
```

```
P1=Pressures_1(1);
```

```
P2=Pressures_1(2);
```

```
P3=Pressures_1(3);
```

```
P4=Pressures_1(4);
```

```
P5=Pressures_1(5);
```

```
Psj=Pressures_2(2);
```

```
Poj=Pressures_2(1);
```

```
%%%%%%%%%%%%%%
```

```
%Temperature in pipe
```

```
%Tp=is entered manually in the GUI;
```

```
%%%%%%%%%%%%%%
```

```
%%%%%%%%%%%%%%CALCULATIONS%%%%%%%%%%%%%%
```

```
%%%%%
```

```
q_probe=P2-(P1+P3)/2;
```

```
V_jet(i)=sqrt(1-(Psj/Poj)^((gam_air-1)/gam_air))*sqrt(2*Cp_air*Tp);
```

```
Cp1_Probe(i)=(P2-P1)/q_probe;
```

```
Cp2_Probe(i)=(P2-P3)/q_probe;
```

```
Cp3_Probe(i)=(P1-P3)/q_probe;
```

```
At_Probe(i)=(P2-Poj)/q_probe;
```

```

As_Probe(i)=q_probe/(Poj-Psj);

%Mach Number
Mach_No(i)=sqrt(((Poj/Psj)^((gam_air-1)/gam_air)-1)*(2/(gam_air-1)));

end

%%%%%%%%%%%%%
%Average the values
%%%%%%%%%%%%%
cur_angle=(cur_angle(1)+cur_angle(2)+cur_angle(3))/3;

%q_probe=(q_probe(1)+q_probe(2)+q_probe(3))/3;

Cp1_Probe=(Cp1_Probe(1)+Cp1_Probe(2)+Cp1_Probe(3))/3;

Cp2_Probe=(Cp2_Probe(1)+Cp2_Probe(2)+Cp2_Probe(3))/3;

Cp3_Probe=(Cp3_Probe(1)+Cp3_Probe(2)+Cp3_Probe(3))/3;

V_jet=(V_jet(1)+V_jet(2)+V_jet(3))/3;

At_Probe= (At_Probe(1)+At_Probe(2)+At_Probe(3))/3;

As_Probe=(As_Probe(1)+As_Probe(2)+As_Probe(3))/3;

Mach_No=(Mach_No(1)+Mach_No(2)+Mach_No(3))/3;

Tj=Tj;

%Create the data array to be written.
m=[cur_angle, Pressures_1(1),Pressures_1(2),Pressures_1(3), Pressures_1(4),
Pressures_1(5),Pressures_2(2),Pressures_2(1), Tp, Tj, q_probe, V_jet,
Cp1_Probe, ...
Cp2_Probe, Cp3_Probe, At_Probe, As_Probe, Mach_No];

%Freddy.txt is a notepad value used to hold on to data outside of the
%program to ensure headers will be created.
load freddy.txt

%restart.txt is a notepad value used to hold on to data outside of the
%program to ensure data will not be overwritten if the run is restarted.
load restart.txt

```

```

a=freddy+1+restart;

%create a variable that can be evaluated so that the values of lines
%can be changed.

fred = ['ExcelWrite(' "C:\Documents and Settings\user\Desktop\Five
Hole Probe\Calibration\testing1.xls'", 0,'...
"" '[' num2str(a) ',' num2str(2) ']' "", ', m')];

%evaluate the variable and send the info to ExcelWrite to evaluate it and
%send it to an EXCEL Spreadsheet.
eval(fred);

%Change the value of freddy to next row number.
freddy=freddy+1;

%Save the row number to a text file so that it will not be cleared.
save freddy.txt freddy -ascii

```

APPENDIX D – OPEN-THROTTLE RAW DATA

APPENDIX D-1 – 30% DESIGN SPEED

position	P1	P2	P3	P4	P5	Psj	P0j	
30%	0.109	100615.3	100025.4	99999	100516.5	100474.5	99795.24	100705.4
	0.094	100613.6	99999.58	99929.63	100519.1	100458.3	99796.08	100712.1
	0.079	100610.3	99980.43	99904.52	100510.6	100460.8	99802.8	100666.4
	0.066	100609.8	99973.77	99838.98	100500.5	100462.4	99801.12	100641.7
	0.053	100608.6	99941.31	99820.68	100491.6	100449.1	99796.92	100655.1
	0.042	100587.5	99927.16	99783.23	100453.3	100440.8	99787.67	100648
	0.031	100606	99950.05	99826.21	100472.2	100459.5	99796.08	100629.5
	0.022	100607.7	99946.72	99824.08	100483.6	100451.6	99798.18	100689
	0.014	100606	99979.18	99881.11	100488.3	100453.7	99794.82	100677.7
	0.008	100559.6	99981.68	99878.13	100471.4	100408.3	99806.16	100663.9
	0.003	100438.5	99927.99	99851.32	100387.9	100237	99796.92	100630.4
	0.001	100373.5	99942.56	99924.52	100347.4	100109.5	99797.34	100662.6
	0.000	100275.2	99992.5	99992.62	100282	99889.13	99809.94	100680.7

APPENDIX D-2 – 40% DESIGN SPEED

angle	P1	P2	P3	P4	P5	Psj	P0j	
40%	0.000	99438.23	98894.92	98918.43	99402.78	98780.02	98594.95	100396.9
	0.002	99578.35	98839.56	98785.22	99521.75	99091.25	98582.77	100289.2
	0.003	99734.08	98830.4	98659.68	99625.95	99371.66	98565.12	100186.9
	0.008	99952.28	98895.33	98715.43	99774.46	99669.56	98581.51	100114
	0.014	100022.3	98902.41	98733.73	99817.91	99749.97	98570.59	100073.7
	0.022	100024.5	98801.68	98647.33	99793.44	99745.39	98543.7	100068.7
	0.031	100023.6	98866.61	98587.33	99786.27	99756.64	98586.55	100104.3
	0.041	100025.7	98848.3	98531.15	99809.47	99746.22	98586.97	100114
	0.054	100045.1	98820.83	98646.91	99843.64	99750.39	98589.07	100090.5
	0.066	100039.2	98856.21	98674.57	99839	99735.8	98575.21	100067.4
	0.079	100043.9	98920.31	98699.68	99842.8	99761.22	98591.17	100075
	0.094	100038.4	98971.92	98782.25	99858.83	99765.38	98586.97	100036.8
	0.109	100026.6	98995.23	98889.07	99845.75	99760.38	98602.93	100068.7

APPENDIX D-3 – 50% DESIGN SPEED

angle	P1	P2	P3	P4	P5	Psj	P0j	
50%	0.109	99362.26	97831.05	97633.58	99087.64	98976.68	97169.9	99725.83
	0.094	99347.91	97756.12	97451.43	99069.07	98935.85	97153.1	99597.99
	0.079	99339.04	97657.48	97330.14	99055.15	98915.01	97132.09	99478.95
	0.066	99347.48	97610.45	97250.13	99044.18	98924.18	97132.51	99384.22
	0.053	99351.71	97585.89	97201.61	99024.36	98922.51	97137.55	99407.69
	0.042	99339.47	97511.8	97099.9	99015.5	98907.93	97118.23	99389.25
	0.031	99347.06	97542.18	97174.8	99009.59	98930.43	97167.38	99380.86
	0.022	99312.03	97511.8	97205.87	98960.65	98920.01	97132.09	99368.71
	0.014	99328.91	97634.17	97349.29	99013.81	98933.76	97160.24	99419.85
	0.008	99265.18	97589.63	97399.08	99006.21	98824.18	97168.64	99408.53
	0.003	98995.07	97545.93	97308.01	98795.7	98447.12	97160.24	99393.02
	0.001	98679.38	97530.95	97466.33	98561.98	97946.31	97174.94	99363.68
	0.000	98465.4	97616.69	97641.67	98402.08	97490.92	97143.44	99353.2

APPENDIX D-4 – 60% DESIGN SPEED

angle	P1	P2	P3	P4	P5	Psj	P0j	
60%	0.000	97257.91	96072.91	96110.4	97161.76	95933.09	95436.91	98868.24
	0.002	97549.12	95946.38	95823.98	97384.51	96570.14	95424.3	98750.88
	0.003	97893.52	95920.16	95603.53	97623.72	97164.27	95422.62	98623.45
	0.008	98459.91	96101.21	95767.38	98076.39	97857.15	95430.18	98592.02
	0.014	98540.52	96112.87	95779.72	98106.35	97969.23	95445.31	98607.94
	0.022	98538.41	96021.3	95462.23	98037.58	97967.98	95431.02	98576.09
	0.031	98578.09	95988.83	95489.9	98073.44	97978.4	95420.94	98568.13
	0.041	98558.67	95974.26	95486.92	98094.11	97957.15	95449.51	98576.93
	0.054	98529.55	96053.35	95529.05	98047.71	97935.48	95411.28	98573.16
	0.066	98572.6	96121.61	95663.54	98130.82	97966.31	95456.23	98606.69
	0.079	98540.52	96183.21	95754.19	98113.1	97937.15	95450.77	98574.83
	0.094	98551.92	96295.17	95930.81	98159.5	97984.23	95427.24	98565.61
	0.109	98548.96	96400.06	96028.27	98167.94	98006.73	95404.14	98513.64

APPENDIX D-5 – 70% DESIGN SPEED

position	P1	P2	P3	P4	P5	Psj	P0j	
70%	0.001	97641.55	94703.53	94379.96	97118.73	96927.2	93382.1	98003.53
	0.003	97590.06	94571.17	94018.21	97038.15	96841.79	93342.61	97724.37
	0.008	97603.99	94401.77	93845	97009.04	96815.12	93355.21	97707.18
	0.014	97609.9	94313.11	93669.66	97035.2	96783.04	93377.48	97577.67
	0.022	97585.84	94257.34	93448.78	96973.6	96755.54	93376.22	97640.96
	0.031	97582.04	94119.56	93378.13	96923.82	96767.21	93347.23	97550.84
	0.041	97600.62	94175.34	93308.76	96904.42	96820.54	93341.35	97550.84
	0.053	97555.03	94166.6	93410.47	96859.7	96801.37	93364.45	97566.35
	0.067	97555.03	94396.77	93584.96	96945.34	96811.37	93349.33	97613.29
	0.079	97433.9	94258.58	93797.76	96905.26	96629.72	93355.21	97627.96
	0.094	96827	94054.22	93612.63	96456.8	95827.68	93312.78	97607.43
	0.109	96270.73	94104.58	93902.45	96050.11	94944.81	93389.66	97548.74

APPENDIX D-6 – 80% DESIGN SPEED

position	P1	P2	P3	P4	P5	Psj	P0j	
80%	0.000	94282.87	92170.38	92215.42	94069.81	92152.04	91115.55	96893.61
	0.002	94959.84	92104.62	91804.3	94668.04	93295.73	91152.1	96782.11
	0.003	95584.05	91906.91	91612.36	95081.48	94254.42	91147.48	96727.62
	0.008	96355.14	92331.88	91508.1	95694.89	95294.79	91094.54	96677.74
	0.014	96523.54	92198.27	91622.58	95727.37	95532.69	91125.21	96600.62
	0.022	96542.11	92030.11	91343.39	95659.03	95550.19	91101.68	96585.53
	0.031	96558.99	92085.89	91151.03	95694.05	95526.44	91113.45	96578.4
	0.041	96537.05	92093.8	91227.63	95680.97	95515.19	91136.97	96551.16
	0.054	96579.67	92235.73	91316.16	95766.61	95516.03	91115.55	96548.64
	0.066	96605	92366.84	91542.14	95850.56	95547.27	91090.34	96627.86
	0.079	96596.13	92532.91	91738.34	95863.22	95570.19	91142.01	96587.21
	0.094	96576.72	92642.38	92009.01	95867.02	95599.77	91131.51	96573.79
	0.109	96617.66	92882.54	92304.8	95945.49	95705.18	91144.12	96562.06

APPENDIX D-7 – 90% DESIGN SPEED

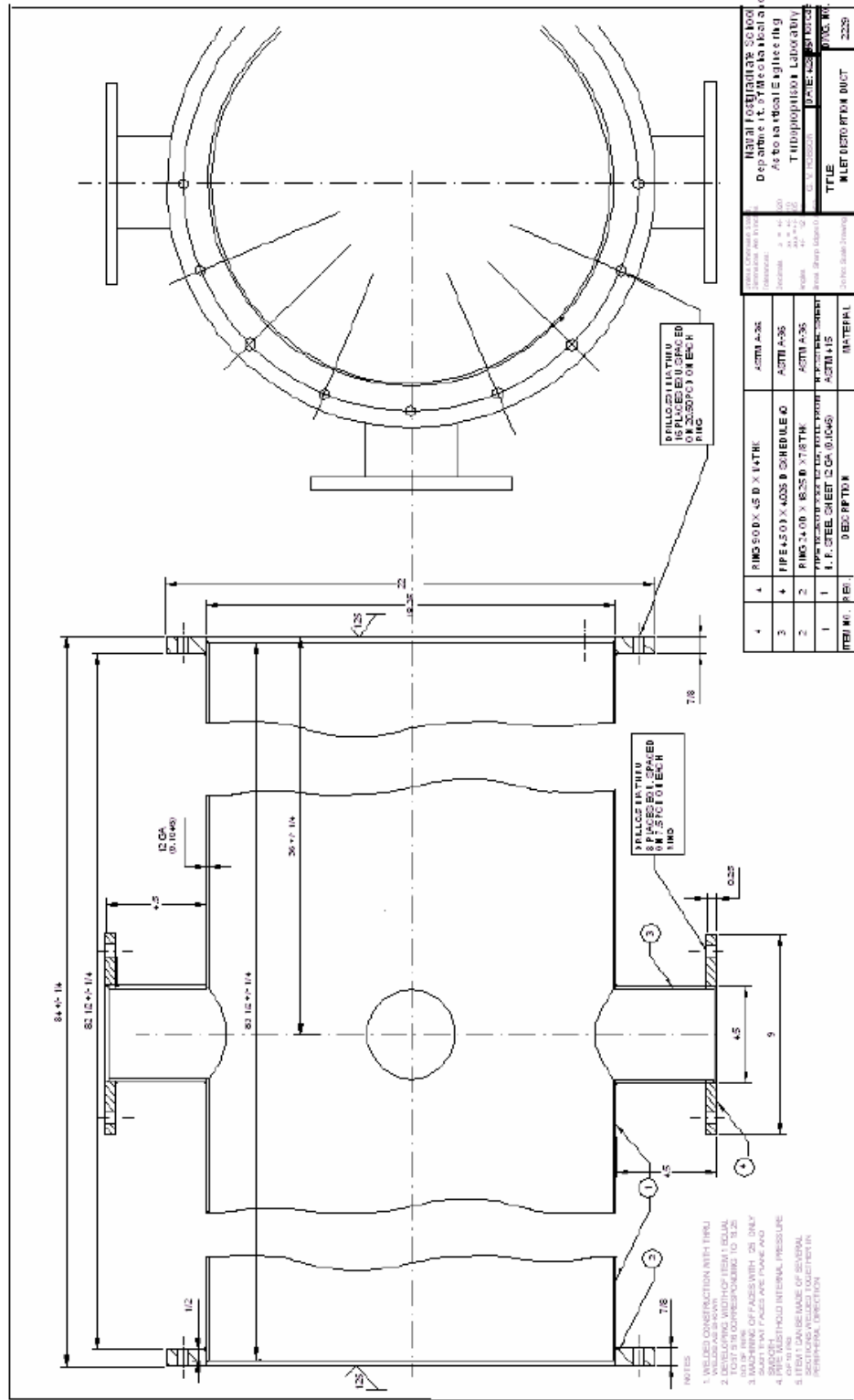
	position	P1	P2	P3	P4	P5	Psj	P0j
90%	0.109	95684.92	91195.58	90524.56	94876.02	94571.07	89025.03	96010.03
	0.095	95673.11	90938.36	90165.37	94825.82	94486.08	89002.34	95713.27
	0.079	95652	90718.59	89689.56	94746.51	94428.17	88996.04	95643.27
	0.066	95590.39	90406.42	89500.6	94643.99	94321.5	88983.86	95601.78
	0.053	95626.26	90304.86	89340.58	94624.16	94343.59	88973.77	95638.66
	0.041	95671.84	90310.69	89124.8	94673.52	94403.58	89014.1	95592.97
	0.031	95668.89	90245.76	89078.84	94619.94	94419.42	89004.44	95634.47
	0.022	95616.55	90226.19	89139.7	94582.4	94404.42	88981.75	95605.55
	0.014	95578.57	90477.59	89506.98	94599.69	94388.17	89018.73	95636.98
	0.008	95461.66	90487.58	89622.74	94640.61	94176.93	89069.56	95647.88
	0.003	94469	89967.72	89479.32	93855.08	92890.75	89032.59	95598
	0.001	93660.77	89944.41	89824.04	93275.42	91724.14	89004.44	95582.08
	0.000	92813.29	90331.5	90359.43	92574.68	90235.47	89008.64	95564.89

APPENDIX D-8 – 100% DESIGN SPEED

	position	P1	P2	P3	P4	P5	Psj	P0j
100%	0.000	91428.54	88410.2	88529.83	91122.15	88357.65	86947.53	95027.54
	0.002	92364.65	88147.98	87953.58	91979.83	90005.48	86976.52	94848.14
	0.003	93444.68	88020.2	87436.92	92710.1	91585.4	86908.04	94763.05
	0.008	94466.46	88608.74	87406.7	93504.07	92956.99	86943.33	94749.64
	0.014	94651.32	88259.95	87579.49	93495.64	93220.73	86941.23	94631.02
	0.022	94737.42	88338.2	87231.36	93507.87	93305.72	86934.09	94647.36
	0.031	94688.04	88242.88	87191.36	93449.23	93242.39	86921.9	94707.72
	0.041	94728.98	88397.72	87220.72	93567.78	93256.14	86989.96	94755.5
	0.054	94754.72	88583.35	87289.24	93632.75	93254.89	87022.31	94735.8
	0.066	94744.59	88769.41	87459.48	93632.33	93263.64	87010.55	94675.87
	0.079	94742.91	88929.65	87805.05	93687.59	93306.97	86945.01	94686.34
	0.094	94737.42	89181.47	88206.81	93716.28	93372.8	86935.35	94737.9
	0.109	94743.33	89409.98	88640.91	93761.84	93461.97	86969.38	94733.71

THIS PAGE INTENTIONALLY LEFT BLANK

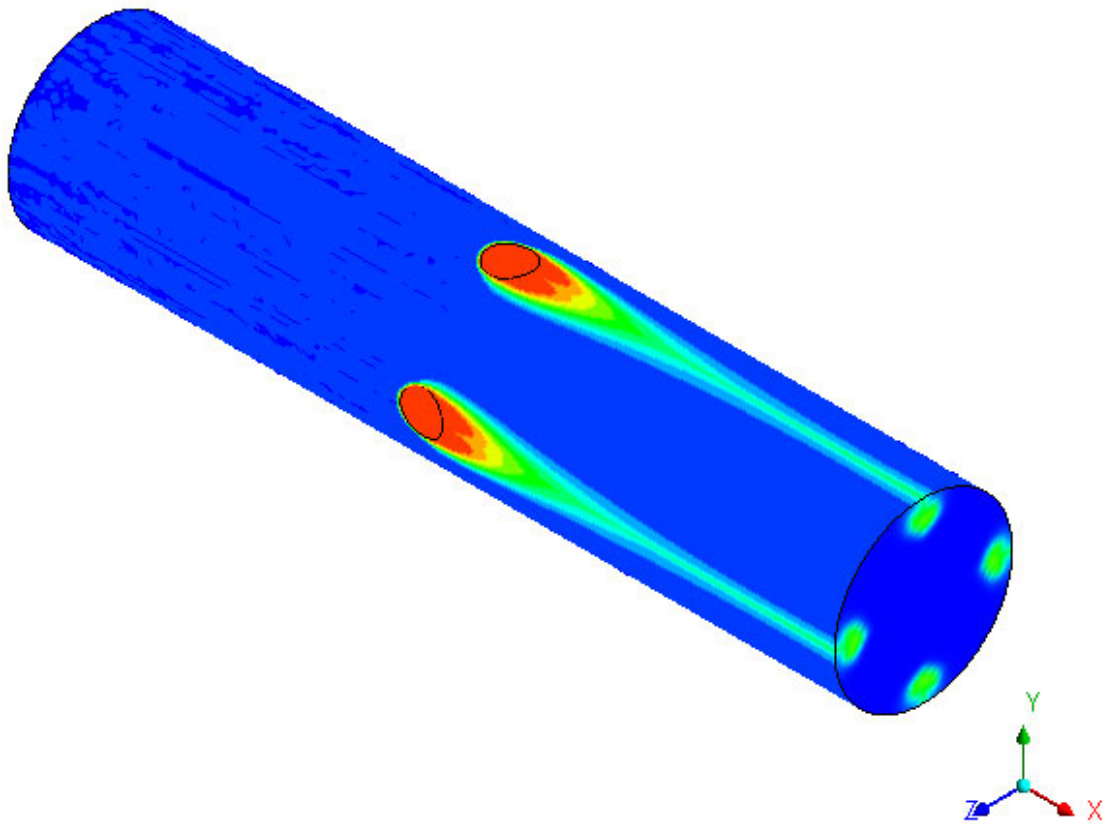
APPENDIX E – INLET DISTORTION SCHEMATIC



THIS PAGE INTENTIONALLY LEFT BLANK

APPENDIX F – MULTI-PHASE FLOW EXAMPLE

CFX



The first step in developing two-phase flow using CFX was to create a model where every surface had its own boundary region. Next each region was designated with a specific type of boundary condition, for this example all four injectors were an “INLET” condition, however they could easily be defined as “WALL” conditions in order to limit their use. Next, in the general mode, the domain of the entire model was edited. In the domain settings the specific fluid can be defined. For multi-phase flow, both ideal gas air and steam at 100°C were selected by holding the “CTRL” key while selecting the fluid models. Next each boundary condition was defined as in any other model, however for inlet conditions there was an additional tab for volume

ratio. At each inlet the ratio of air volume and steam volume can individually be defined; for this example the air inlet had an air volume ratio of 1 and a steam volume ratio of 0, and vice-versa for the steam injector inlets. The specific boundary conditions used to create the results pictured above were 30m/s, 100% air flow into the main duct inlet and 10m/s, 100% steam flow into each of the four injectors.

INITIAL DISTRIBUTION LIST

1. Defense Technical Information Center
Ft. Belvoir, Virginia
2. Dudley Knox Library
Naval Postgraduate School
Monterey, California
3. Distinguished Professor and Chairman Anthony Healey
Department of Mechanical and Aeronautical Engineering
Naval Postgraduate School
Monterey, California
4. Professor Ray Shreeve
Department of Mechanical and Aeronautical Engineering
Naval Postgraduate School
Monterey, California
5. Professor Garth Hobson
Department of Mechanical and Aeronautical Engineering
Naval Postgraduate School
Monterey, California
6. Dr. Anthony Gannon
Department of Mechanical and Aeronautical Engineering
Naval Postgraduate School
Monterey, California
7. ENS Matthew D. Brunner
Monterey, California